Advances in Applied Energy 10 (2023) 100138

Contents lists available at ScienceDirect

Advances in Applied Energy

journal homepage: www.elsevier.com/locate/adapen

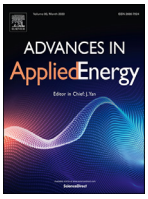

TOM.D: Taking advantage of microclimate data for urban building energy modeling

Thomas R. Dougherty*, Rishee K. Jain

Stanford University, 450 Serra Mall, Stanford, 94305, CA, USA

ARTICLE INFO

Keywords:
Urban microclimate
Remote sensing
Machine learning
Land surface temperature
Climate model
Urban heat island

ABSTRACT

Urban Building Energy Modeling (UBEM) provides a framework for decarbonization decision-making on an urban scale. However, existing UBEM systems routinely neglect microclimate effects on building energy consumption, potentially leading to major sources of error. In this work, we attempt to address these sources of error by proposing the large scale collection of remote sensing and climate modeling data to improve the capabilities of existing systems. We explore situations when remote sensing might be most valuable, particularly when high quality weather station data might not be available. We show that lack of access to weather station data is unlikely to be driving existing errors in energy models, as most buildings are likely to be close enough to collect high quality data. We also highlight the significance of Landsat8's thermal instrumentation to capture pertinent temperatures for the buildings through feature importance visualizations. Our analysis then characterizes the seasonal benefits of microclimate data for energy prediction. Landsat8 is found to provide a potential benefit of an 8% reduction in electricity prediction error in the spring and summertime of New York City. In contrast, NOAA RTMA may provide a benefit of a 2.5% reduction in natural gas prediction error in the winter and spring. Finally, we explore the potential of remote sensing to enhance the quality of energy predictions at a neighborhood level. We show that benefits for individual buildings translates to the regional level, as we can achieve improved predictions for groups of buildings.

1. Introduction

Buildings play a prominent role in the conversation of urban decarbonization. Rightly so, as they consume roughly 40% of the electricity supply in the United States. Urban Building Energy Modeling (UBEM) provides a framework for decarbonization decision-making. However, UBEM has limited capacity to accurately model individual building energy and the energy consumption patterns of larger aggregated urban regions [1]. While most of the uncertainty within urban energy modeling seems to be the correct characterization of building features [2,3], a growing body of research is now exploring how a lack of adequate microclimate description may be adversely influencing the quality of models.

Recent work has highlighted existing discrepancies between climate modeling and energy systems [4,5]. The lack of integration between energy models and climate models may be particularly detrimental, considering that the existing tools for UBEM rely on Typical Meteorological Year (TMY) files to represent climate conditions. These files are generated from nearby weather stations, which may or may not be in the same microclimate zones as the simulated buildings. However, given that climate change has a disproportionate impact on urban areas [6], errors caused by the failure to measure urban microclimate are likely to increase as variance in urban temperatures intensifies.

High thermal mass buildings in urban areas additionally opens the opportunity for thermal interactions via longwave radiation, which was estimated to increase cooling demand by up to 3.3% and decrease heating demand by up to 3.6% in Chicago [7]. A separate, simulation-based study in Nanjing, China, found that urban morphology significantly influences urban temperatures and wind speeds. The estimated discrepancy between EPW-based simulations and those inclusive of microclimate was thus estimated to be up to 23% [8]. Shading between buildings provides another effective mechanism for the perturbation of radiative heat transfer, with seemingly trivial decisions often responsible for large inefficiencies. For example, the layout of rooftop units may achieve a 42% efficiency benefit when positioned within shaded regions of the roof [9].

Vegetation, neighboring structures, and impervious surfaces have been shown to substantially impact the operating performance structures by modifying the temperature and climate [10,11]. While wind is less represented in the research for its impact on building energy consumption, high wind speeds modify the heat transfer characteristics of the building with its environment. Preliminary studies have indi-

* Corresponding author.
E-mail address: tomdou@stanford.edu (T.R. Dougherty).

https://doi.org/10.1016/j.adapen.2023.100138
Received 10 March 2023; Received in revised form 12 April 2023; Accepted 16 April 2023
Available online 24 April 2023

cated that wind may increase the energy consumption of a structure by as much as 5% [12]. These works signal the potential benefit of high-resolution urban climate models, which have been a fixture of the research community for the past two decades, starting with urban canopy models [13]. Complex heat transfer interactions are often distilled into a resistive-capacitive (RC) system, which enables the modeler to represent interactions using an electrical equivalence [14,15]. Modern research into urban climates now allows utilities to generate files that may be used for more accurate urban building energy modeling [16].

While work has been conducted to generate utilities for modeling urban microclimate conditions [16–18], typically, it is done so to explore the health consequences of UHI [19], pedestrian comfort [20], or water resources [21]. This work seeks to shed light on the potential benefits of various remote sensing datasets in the context of urban energy modeling.

As a large variety of climatic subterms may contribute to the heat transfer of each structure, we focus the scope of work within this paper on a simple exploration of the utility for each data source without extended conversation as to its physical interaction with the structure. This work therefore addresses a large gap in scientific literature, which is that of the sensitivity between a building's energy consumption and its environmental conditions. A diverse dataset of environmental features from various climate models and satellites provides an array of possible interaction effects, with the rationale that this breadth of sources may help to identify powerful features for deeper integration with physics based modeling. As building energy modeling is famously over-constrained, the current standard for model calibration may incorrectly classify model error from environmental causes as those caused by occupancy behavior or building features. Through the systemic incorporation of any potent datasources discovered in this analysis, future modelers might avoid the potential mistake of overcompensating for microclimate impacts on building energy consumption. Our approach is then bridged to existing concepts from Urban Building Energy Modeling (UBEM) through the use of the popular UBEM metrics CV(RMSE) and NMBE to better understand the order of magnitude for benefit from each data source in a common language.

The overall methodology of this paper follows the outline found in Fig. 1. The data section comprises the content found in phases zero, one, and two. The methods section covers phase three and the results are divided into phases four and five.

The contributions of this work and its relation to larger modeling efforts may additionally be summarized in the following ways:

1. Estimation of value to building energy modeling from various open access data sources.
2. Contextualization of relative temporal benefits of incorporating open access data sources.
3. Scaling behavior of multi-building energy models with the incorporation of auxiliary data sources.
4. A method to enable the interpretation of nonlinear relationships between environmental features and energy consumption.
5. Quantification of potential data degradation from weather stations with diminished spatial relevance to a given building.

Abbreviations Table

UBEM	Urban Building Energy Modeling
SRTM	Shuttle Radar Topography Mission
UHI	Urban Heat Island
RTMA	Real-Time Mesoscale Analysis
CFD	Computational Fluid Dynamics
BES	Building Energy Simulation
ESPG	European Petroleum Survey Group
CMIP	Coupled Model Intercomparison Project
NOAA	National Oceanic and Atmospheric Administration
EPW	EnergyPlus Weather
TMY	Typical Meteorological Year
CV(RMSE)	Coefficient of the Variation of the Root Mean Square Error
MAE	Mean Absolute Error

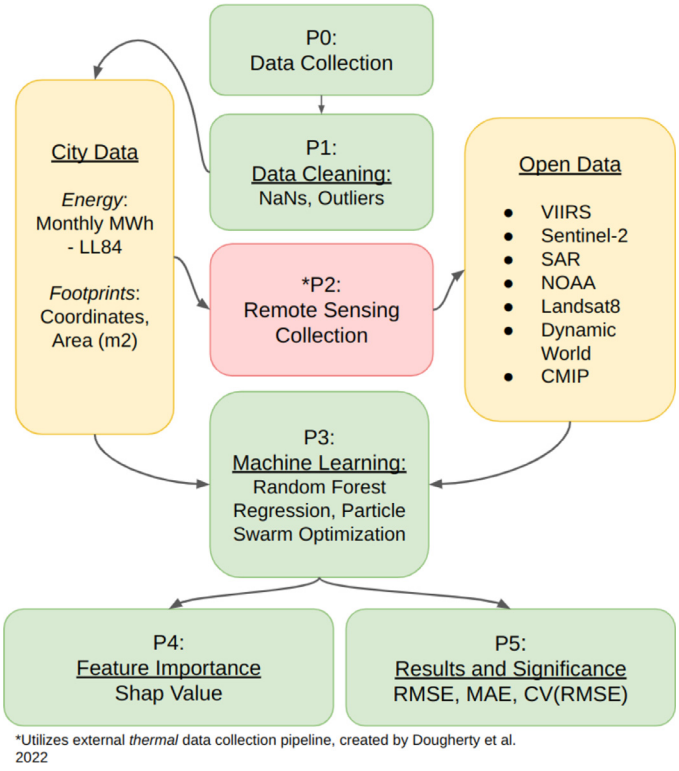

Fig. 1. Flowchart outlining the steps taken throughout the process and intermediate data files created and used for subsequent studies.

Table 1
Schema Data Compression Descriptions.

Schema	Q_5	Q_{25}	Median	Q_{75}	Q_{95}
$\mathbf{S}_1$			✓		
$\mathbf{S}_2$		✓	✓	✓	
$\mathbf{S}_3$	✓	✓	✓	✓	✓

2. Data

This analysis can be considered a regression problem, with the task of predicting the structure's energy consumption. For all data sets used in this study, our goal is the prediction of monthly energy consumption. Therefore although each data set has unique collection frequencies, we coerce our measurements into monthly intervals while attempting to capture pertinent information from the dataset. To accomplish this, we use three different schemas of compressing the data into the monthly format. The schema data compression information can be found in Table 1.

Schema $\mathbf{S}_1$ is the simplest and will be used to interpret model results. In contrast, schema $\mathbf{S}_3$ is expected to have the best performance, as the most information about the data is communicated to the machine learning pipeline.

Underlying the mechanics of compressing data into the monthly domain is the conversation about the importance of two themes for the data. The first is high spatial resolution, the capacity to capture pertinent information directly adjacent to the structure. The second is time resolution, or the data's ability to capture and communicate extreme swings throughout the month. As remote sensing data may only collect 1–5 samples per month over a city, it has low temporal resolution and high spatial resolution. Because of this, schema $\mathbf{S}_1$ may give us insight into the potential relative benefit of high spatial resolution, while the transition to schemas $\mathbf{S}_2$ and $\mathbf{S}_3$ will shed light into the value of high temporal resolution.

2.1. Energy data

New York City provided the energy data required to conduct this study as a result of the ordinance called Local Law 84, which mandates that buildings over 25,000 sq.ft. must report their energy consumption at a monthly resolution. Unfortunately, not all energy sources are represented in this data. Notably for New York, there is an absence of data on steam utilization rates. Electricity and natural gas are the terms reported on the monthly scale, which will be the focus of this analysis.

To control that the months have different numbers of days, we convert the monthly consumption into a daily value by dividing the consumption by the number of days in the month. This serves as the consumption pattern of a typical day in the month, which we choose to use as the predictor.

The energy consumption data is heavily right-skewed, and extreme values are pruned by only considering energy consumption terms between the 2nd and 98th percentiles. There is still substantial unbalance in the data, with average daily electricity (Q_{25} = 0.49MWh, Q_{50} = 0.88MWh, Q_{75} = 1.85MWh, skewness = 3.78) having more significant skewness than natural gas (Q_{25} = 0.27MWh, Q_{50} = 1.21MWh, Q_{75} = 3.27MWh, skewness = 2.93). Summary statistics for energy consumption may be found in Tables A.1 and A.5.

2.2. Building specific data

The building attributes used in this analysis are provided by the building footprints dataset of New York, which provides a geometric representation of the buildings' outlines in geojson format in addition to the height and age of the structure. The geometry of the building is provided in World Geodetic System 1984 format (ESPG 4326), which does not preserve distances when used in traditional measures. Therefore the area of the building was computed by first projecting the buildings into UTM Zone 18N, which uses meters for its coordinate systems and preserves the quality of measures between the longitudes of 78°W and 72°W.

We additionally register information about individual building classes, representing one of three options: Commercial, Residential, or Manufacturing. While these are not used in the training pipeline or for prediction, they allow us to collect an understanding of the model's capacity as it pertains to each building class.

Natural gas consumption is highly seasonal, with most of the gas used in the coldest months between November and March for heating. Of note, buildings in New York City still heavily rely on steam for heat. As such, the electricity and gas consumption are not fully representative of the total energy consumption for the structure.

2.3. Microclimate

The data used in this analysis parallels that found in the study conducted by Dougherty and Jain [22], which collects precision microclimate features in the immediate region around the structure from various remote sensing sources. These sources include Sentinel-1, Sentinel-2, Landsat8, NOAA reanalysis, prospective coupled model intercomparison project (CMIP) data, elevation maps, and nighttime imagery of the city. All data sources were collected by Google Earth Engine, and the resolution matching process between pixel regions captured via satellites and the boundary of the building is handled internally by Google Earth Engine as defined in [22]. The heightened spatial resolution of these data sets therefore provides significant capacity to directly or indirectly measure localized microclimate effects.

The Landsat8 satellite has a dedicated land surface temperature instrument which we used to curate an initial survey of the median land surface temperature of the city, found in Fig. 2. This preliminary temperature distribution motivates our initial intuition that localized temperatures may significantly drive variance within consumption patterns. Recent research further validates this initial intuition, highlighting the potential role of land surface temperatures from Landsat 8 as a key piece to automate the process of building energy modeling [23].

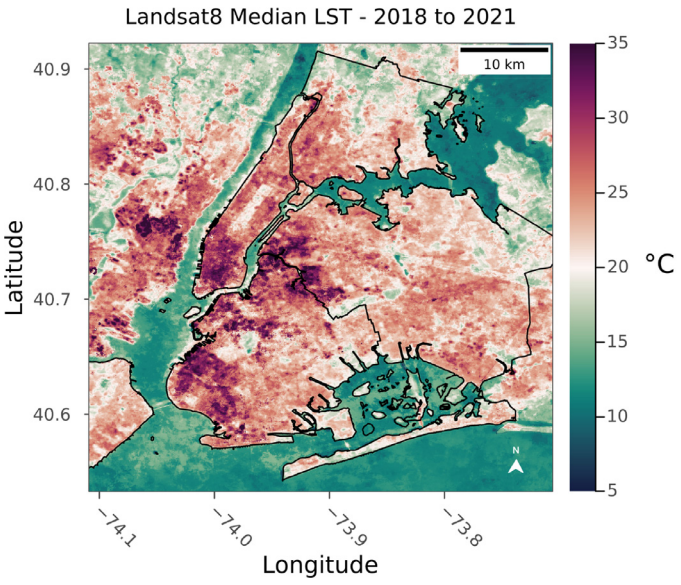

Fig. 2. Median temperature readings for each pixel in New York City over three years, taken by the Landsat8 satellite. Of note, all images were captured from the Landsat instrument between 3:32 PM GMT and 3:41 PM GMT.

Detailed information contained within each dataset and their summary statistics used may be found in a number of tables in the appendix, an example of which for the electricity analysis may be seen in A.1, A.2, and A.3.

2.4. EPW - Motivations and discrepancies

The second data set used in the analysis was curated by extracting environmental features from EnergyPlus Weather (EPW) files which are defined synonymously as TMY files in this analysis. The potential inaccuracies of EPW files, identified by Hong et al. [24], are also identified in New York City. Fig. 3 shows the contrast between measurements taken from the Landsat8 satellite and the expected temperature measurements from the EPW files. The Landsat8 satellite readings are captured between 3 PM and 4 PM GMT, with a median revisit time of 8 days. To calibrate the comparison between the two datasets, we only consider buildings near Central Park which are closest to the Central Park Weather Station (KNYC). We then can filter all readings between 3 PM and 4 PM GMT from the EPW file, and examine the projected dry-bulb temperature of the building based on the EPW file, seen in Fig. 3 as the black line.

For ease of interpretation, a single building is isolated, and its trajectory through the three years is shown with a dark pinkish color. We additionally add the Emissivity Standard Deviation, provided as a Landsat8 Level 2 Collection 1 product, as error bars. Each dot represents the direct value captured at exact dates and times from Landsat8, thus the points are not always aligned to the month. Additionally, inconsistencies in temporal resolution are the cause of natural effects, such as clouds, which may cause a poor quality of data capture and is thus filtered from the study.

Consistent under-measurement of the temperature is characteristic of a strong urban heat island effect, with measurement errors as high as 20 °C in the summer seasons. Given that the energy consumption of buildings is highly coupled to the outdoor air temperature [10], this may already have huge impacts on the cooling loads and

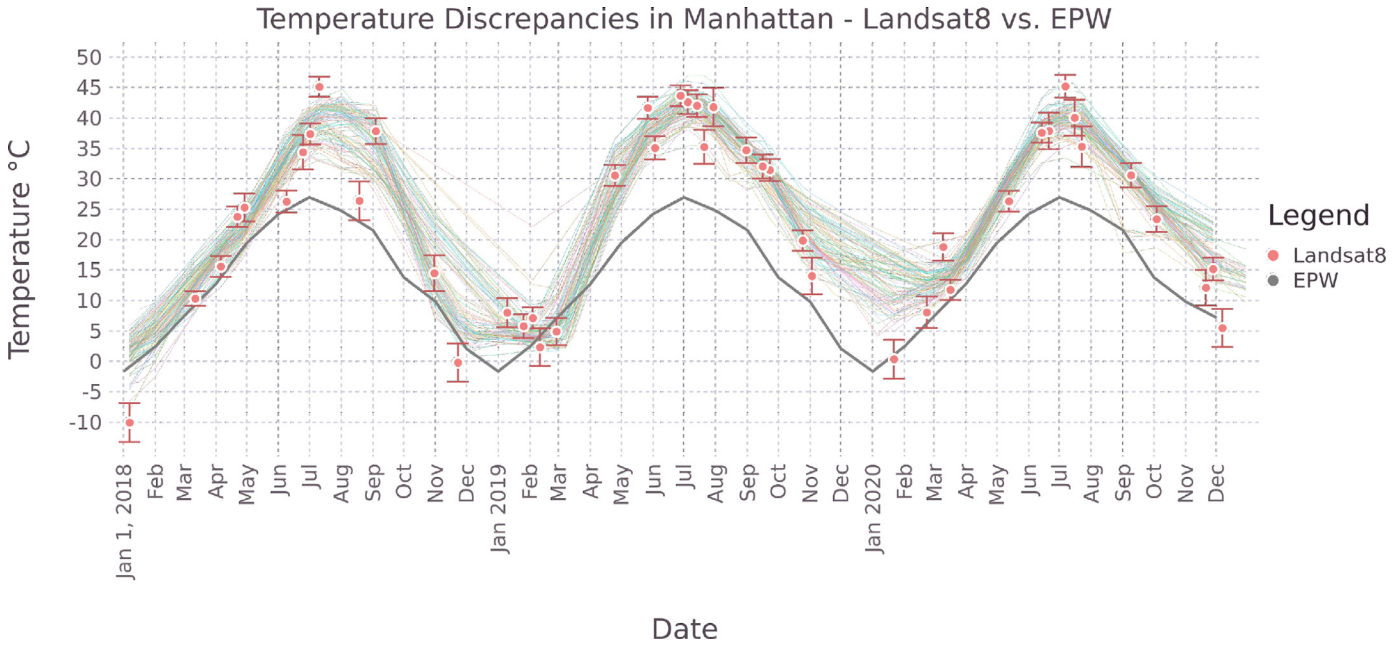

Fig. 3. Temperature Discrepancy between Landsat8 measurements and EPW files. Measurements for a single building at the intersection of E 46th Street and 3rd Street are shown with a dark pinkish color. A random assortment of fifty buildings near Central Park is shown with multicolored lines.

provide a significant source of uncertainty in energy modeling if left ignored.

2.5. EPW - Collection

After establishing motivation for further examining EPW files in our analysis, we constructed a pipeline to collect data from each file and interpret it as part of our machine learning system. To accomplish this, we first constructed a system to identify the nearest weather stations to each building to utilize the most pertinent weather station for each building. A comprehensive data set of available weather stations in the United States is provided by NREL [25], which contains not only the location of each weather station in the United States but an associated EPW file curated from historical weather data at the station. The data types are mapped according to the specification laid out in Chapter 2 of the EnergyPlus "Auxillary Programs" documentation, titled "Weather Converter Program."

A set of candidate weather stations were curated by first computing the centroid of all buildings in the analysis and projecting a uniform radius of 45km around this centroid. This radius is chosen based on the area of New York City, which is recorded to be roughly 783.8 sq.km, and on visible inspection to confirm that the radius adequately captures all data points. The distance between each point and each weather station is then computed, with the smallest distance serving as an indicator of the mapping between the building and the weather station. Given that prior research has employed a similar distance metric to curate a high-resolution model of urban climate [24], this is an appropriate method of mapping buildings to weather stations.

Projected back onto a map in Fig. 4, weather stations in the city's center have excellent coverage of Manhattan, the Bronx, and Queens. However, Staten Island and Brooklyn have notably higher average distances to the nearest weather station.

The time resolution of the EPW files used in this analysis is hourly. To capture the profiles of each weather variable without the redundancy of data associated with hourly weather for each building, we aggregated statistics about each building by compressing daily values into maximum, median, and minimum terms. Therefore for each day we have three values for each variable to express the variability of the term throughout the day.

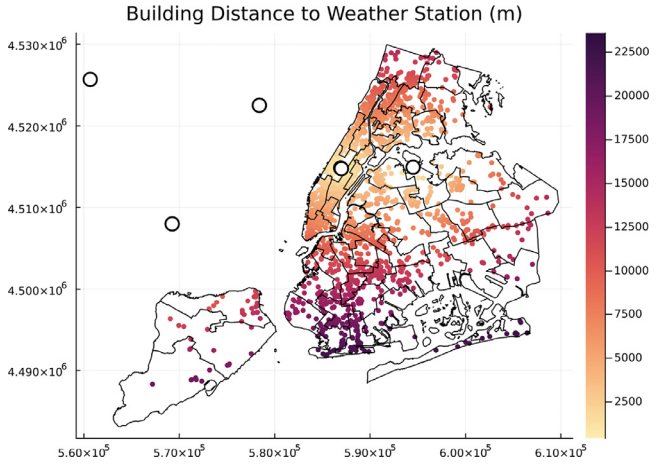

Fig. 4. Distance between each building and the closest weather station, measured in meters. The map projection is UTM Zone 18N; thus the gridline differences are measured in meters.

3. Methods

3.1. Model

As this work focuses not on the model selection but on the data quality, the model architecture and endogenous terms remain static while the exogenous data is modified to reflect the utilization of a new data source. This permits conversation on data quality which exists in isolation from the quality of the model. Random Forest regressors are chosen to reduce the amount of preprocessing associated with the data, as random forest models do not require normalization prior to prediction. Additionally, prior work has validated the benefit of decision trees, which live at the heart of random forest regression, for the task of predicting building energy consumption [26]. The EvoTrees.jl package was used as an interface to random forest regression for its support with graphics processing units, which was utilized through its interface in the MLJ package [27].

3.2. Training pipeline

In splitting our data, we seek to avoid the overfitting of a building against its historical data. To avoid overfitting, we do not split by unique data points, which capture the monthly energy consumption of a given structure, but instead split the data by buildings. After aggregating all terms for electricity and natural gas into standard datasets and removing missing data, 9483 buildings are represented in the electricity data and 8891 buildings are contained in the final natural gas dataset.

The test dataset is composed by randomly selecting 20% of the buildings, amounting to 1701 structures for electricity and 1584 buildings for natural gas. The training sets are therefore composed of 7782 buildings for electricity and 7229 buildings for natural gas. With an average of about 24 samples per building represented in the data for both datasets, 189,625 unique data points exist for electricity and 172,213 data points exist for natural gas within this three-year window.

To determine the appropriate hyperparameters for each dataset, cross-validation was used by splitting against the buildings in the training dataset. Each cross-validation set was composed of 475 buildings for both electricity and natural gas. The RMSE is the loss function for training, defined in Eq. (1).

$$\textbf{RMSE} = \sqrt{\frac{\sum_{i=1}^{n}(\hat{y}_i - y_i)^2}{n}} \tag{1}$$

Fifteen folds were used, with the RMSE calculated for each fold and averaged into a single value. This process happens for each set of hyperparameters. A tuning engine was constructed using the Adaptive Particle Swarm optimization scheme, which uses inspiration from genetic algorithms to converge on a generally optimal set of hyperparameters [28]. This tuning process comprised 75 unique trials within the domain of possible hyperparameter permutations for the random forest. Some data sets have significantly more parameters than others, which in turn impacts the hyperparameters of each model as the particle swarm optimization balances bias and variance. While we attempt to build consistency by only using Random Forest Regressors, this hyperparameter tuning for each data source introduces nuanced differences to each model. Thus for the rest of this analysis, references to a data set's model will simply imply that the Random Forest Regression with Particle Swarm Optimization was conducted against the source of data, selecting unique hyperparameters for it.

3.3. Validation metrics

The standard validation metrics used in this analysis parallel those portrayed in ASHRAE Guideline 14 [29]. Three metrics are used to establish the quality of a building energy model:

$$\textbf{CV(STD)} = 100 \cdot \frac{\sqrt{\frac{\sum_{i=1}^{n}(y_i - \bar{y})^2}{(n-1)}}}{\bar{y}} \tag{2}$$

$$\textbf{CV(RMSE)} = 100 \cdot \frac{\sqrt{\frac{\sum_{i=1}^{n}(y_i - \hat{y}_i)^2}{(n-p)}}}{\bar{y}} \tag{3}$$

$$\textbf{NMBE} = 100 \cdot \frac{\sum_{i=1}^{n}(y_i - \hat{y}_i)}{(n-p)\bar{y}} \tag{4}$$

The same ASHRAE document outlines the standard of quality for monthly computer simulations of building energy consumption, with **NMBE** $\leq 5\%$ and **CV(RMSE)** $\leq 15\%$.

3.4. Model interpretation

After the model has achieved a relative level of accuracy in prediction, we want to understand better how we might explore the role of each variable in making an accurate prediction. To do this, we utilize an approximation for Shapely values for complex, nonlinear models [30,31].

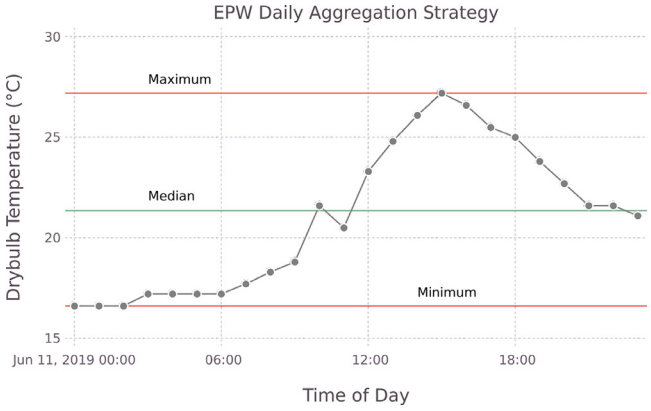

Fig. 5. Process of Aggregating terms from the hourly EPW file into three representative points. Seen here is an example of this process on the drybulb temperature for a typical day in June.

Shapely values originate from game theory [32], with the original task of optimally allocating resources to members of a cooperative team based on their contribution to the team's success. Extending the idea to statistical models allows us to explore how each variable may play a role in the final prediction relative to a mean prediction with typical values. For this analysis, the shapely values in this study provide an insight into how the magnitude of a variable is likely to impact the daily energy consumption of a standard building in the New York City dataset in MWh. Negative values imply that the term is likely to decrease energy consumption, while positive terms indicate that the building is likely to experience an increase in energy consumption.

4. Theory/Calculation

Three research questions are explored in this study to give better insights into the particular benefits of microclimate data for Urban Building Energy Models.

1. How does distance from the nearest weather station impact prediction quality?
2. Does remote sensing have a seasonality of benefits?
3. How might aggregated predictions benefit from remote sensing?

To better contextualize the quality of our results, a Null model is used for every scenario and is composed simply of building features without microclimate data. This null model may provide insight into the existing benefits of EPW data. Additionally, the null model may help contextualize the additional improvements possible through remote sensing (Fig. 5).

4.1. Weather station distance

Given that building energy consumption is quite sensitive to temperature fluctuations, inaccurate measurements of the building's experience may drive significant errors. We explore the relationship between the quality of predictions which are possible with greater distances from the nearest weather station to a building.

In pursuing this research question we predict the energy consumption of all buildings in our test set and examine their relative prediction quality compared to the null model at a discrete set of distances from the nearest weather station.

4.2. Seasonal benefits of remote sensing

The question of seasonal benefits was inspired by the inconsistent relationship between typical EPW readings and the seasonality of the urban heat island (UHI) effect, demonstrated in Fig. 3. In this section, we explore potential seasonal benefits provided by remote sensing.

To explore this research question, the seasonal benefits of each model are calculated by comparing the typical prediction losses for each month, using mean absolute error, to that of the baseline model. The baseline model used in this section is selected as the model trained against the EPW data, which is meant to provide the most realistic reflection of real-world modeling. The average difference in prediction for the model, measured as the average MAE across all predictions for the month, is defined as δ_m. This error is then compared to the average baseline error for the month, which uses the same process to procure a baseline error for each month δ_b. The relative difference between these error profiles, defined as $\Delta_m = 100 \cdot (\frac{\delta_m - \delta_b}{\delta_b})$, is used to gauge the relative benefit of the new model compared to the baseline. Negative values indicate an improvement compared to the baseline, while positive values indicate that the model's error has increased relative to the baseline.

4.3. Aggregated prediction quality

So far, this analysis has focused on the quality of predictions available on the individual building scale in New York. However, some applications in energy modeling instead require the aggregate consumption of a neighborhood or city [33]. While single building energy prediction has its merits in modeling retrofit scenarios [34], research into energy storage requirements on the urban scale often abstracts the region into a single node representing the aggregated energy demand [35–37]. Typically past research hints at the potential relationship between a reduction in error with regional predictions [38]. This study instead follows a similar process to that of Streltsov et al. [39] by formalizing the potential error trajectory of aggregated energy models of various sizes.

In an effort to study aggregation effects, we first use the same models trained against individual buildings, both the null model using only building features and the microclimate models which incorporate data from open access data sources. Individual predictions against buildings may be summed by region within the city, simulating an energy model for a number of buildings within a district of the city. The sum of these predictions may be compared to the sum of the recorded monthly values, which enables us to understand how the common error metrics from UBEM might scale as more buildings are included in this energy analysis. The individual building predications may be built using the null model, without any microclimate information, or through one of the models which incorporates microclimate data. The formal process taken is seen in Eq. (5).

$$AE[j] = \sum B[j] \mid (B \in Z, j \in 1 \dots 12) \tag{5}$$

The zipcode of the building, Z, is used to aggregate a set of buildings contained within the zipcode B. The zipcode was selected as a convenient utility to organize buildings into groups of various sizes. Equation (5) outlines the process of summing the predictions and measurements for each building in the zipcode at each timestep, j. As our timestep is limited to that of the reported monthly energy consumption, the temporal resolution of the data is also on the monthly scale. We use the same validation metrics found in 3.3 for each region.

5. Results

Our results for individual building prediction can be found in Table B.21. One of the more intuitive metrics, RMSE, highlights the significant benefit of including particular microclimate data sets in urban energy models. In particular we see that the inclusion of Landsat8 data and NOAA reanalysis data has a substantial reduction in model RMSE. We also highlight challenges associated with the spatially homogeneous nature of a single city with heterogeneous energy sources, which are likely driving our validation metrics to higher numbers than other studies on the urban scale [40]. The CV(STD) values are included in Table B.21 to remind the reader that the same data was used for each model.

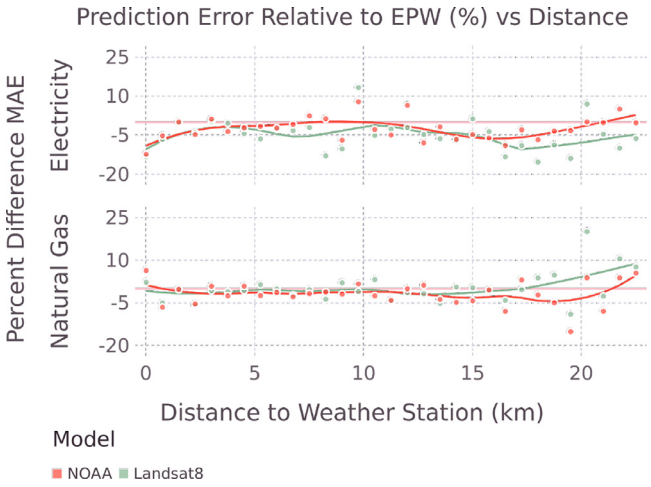

Fig. 6. S_3 error at various distance intervals away from the nearest weather station, measured as a percent difference to the EPW model with negative values indicating an improvement. Dots represent individual measurements for each error percent relative to the baseline EPW model, with the smooth lines showing the trend profile of the predictions. Pink horizontal lines are also shown to highlight the zero benefit scenario, or the EPW model compared to itself.

5.1. Weather station distance

The results of our predictions for individual buildings against their respective distance to the nearest weather station can be found in Fig. 6. Two datasets are highlighted based on their prominence for improved energy prediction overall: Landsat8 and NOAA.

Fig. 6 highlights the benefits of improved spatial resolution data compared to the EPW file. However, due to a lack of apparent downward trends, we cannot confidently make a statement about improvements to predictive performance relative to the EPW file related to weather station distance. Poor predictions around the 20km mark may be an artifact of the New York City data and less telling of EPW failures. The buildings with a minimum weather station distance of more than 20km can be seen on 4, which are often older and may be experiencing unusual coastal weather effects.

5.2. Seasonal benefits

The seasonal benefits for two of the highest performing annual models from B.19, NOAA and Landsat8, can be found in Fig. 7. Only the positive monthly contributions are shown, with each zero value indicating that the EPW model had better performance for this month.

Landsat8 provides substantial opportunities for improved electricity prediction. Particularly between April and October, Landsat8 will likely offer a relative improvement of anywhere between 5% and 10%. NOAA provides the most substantial benefit for natural gas prediction, with most of this benefit occurring in the year's coldest months. For New York City, the winter and Spring months are between December and May. As natural gas is more heavily used for heating, NOAA is likely more accurate than EPW for predicting gas consumption due to freezing temperatures.

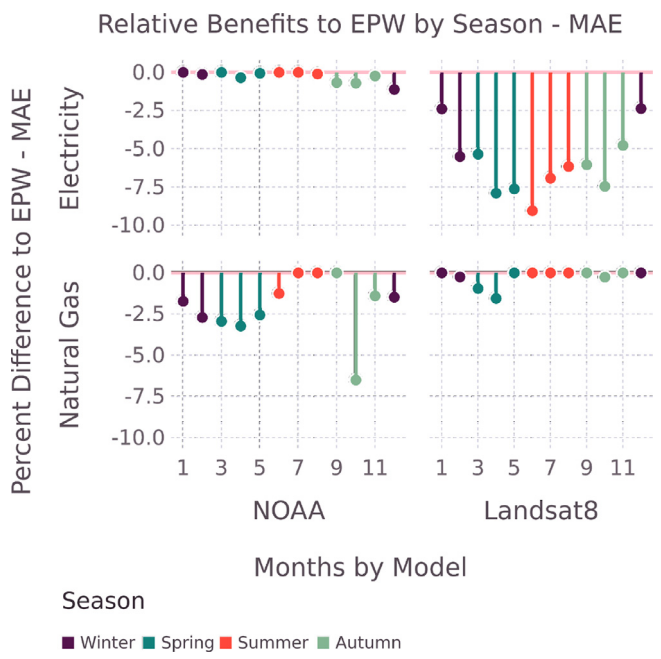

Fig. 7. $\mathbf{S}_3$ monthly average MAE relative to EPW. Only the improved prediction months are shown. The seasons listed here are defined for the northern hemisphere.

5.3. Aggregated benefits

The results of the aggregated analysis from $\mathbf{S}_3$ are found in Table B.24. Summary statistics for the number of buildings in each group is as follows: Group size summary statistics: $Q_{25} = 3$, $Q_{50} = 6$, $Q_{75} = 12$. We find a substantial benefit in utilizing Landsat8 data for electricity prediction and NOAA data for natural gas prediction. We find that the inclusion of Landsat8 as a feature may have the capacity to improve CV(RMSE) predictions by 2.5 and NMBE by around 3.7 compared to EPW files. The inclusion of NOAA data seems to have the capacity to improve natural gas CV(RMSE) by 1.8 and NMBE by 2.5.

We now attempt to understand the relationship between the number of buildings in a set and the metrics computed against them. Fig. 8 visualizes the relationship between the number of buildings on the x-axis and the error metrics on the y-axis. We see a rapid decrease of CV(RMSE) and NMBE with additional buildings in each set, which aligns with findings from prior research [38]. Of note is how rapidly these metrics drop, as most of the reduction compared to the individual building comes with less than ten buildings in a group.

5.4. Feature importance & model interpretation

We again focus on the top-performing models for interpreting model results: Landsat8 and NOAA. Due to the length required to properly highlight the significance of features from a single model, this section will only focus on explaining the potential benefits of Landsat8 for electricity prediction and NOAA for natural gas prediction.

5.4.1. Electricity

Fig. 9 highlights the top ten statistically significant features for making electricity predictions using the Landsat8 dataset. The most significant by far are the building-specific terms. This matches our intuition as we were unlikely to see deviations between models of more than 5%. Among the Landsat8-specific terms, we see that they are dominated by readings associated with Landsat8's thermal instruments indicating that this suite of sensors is what was responsible for its high level of performance.

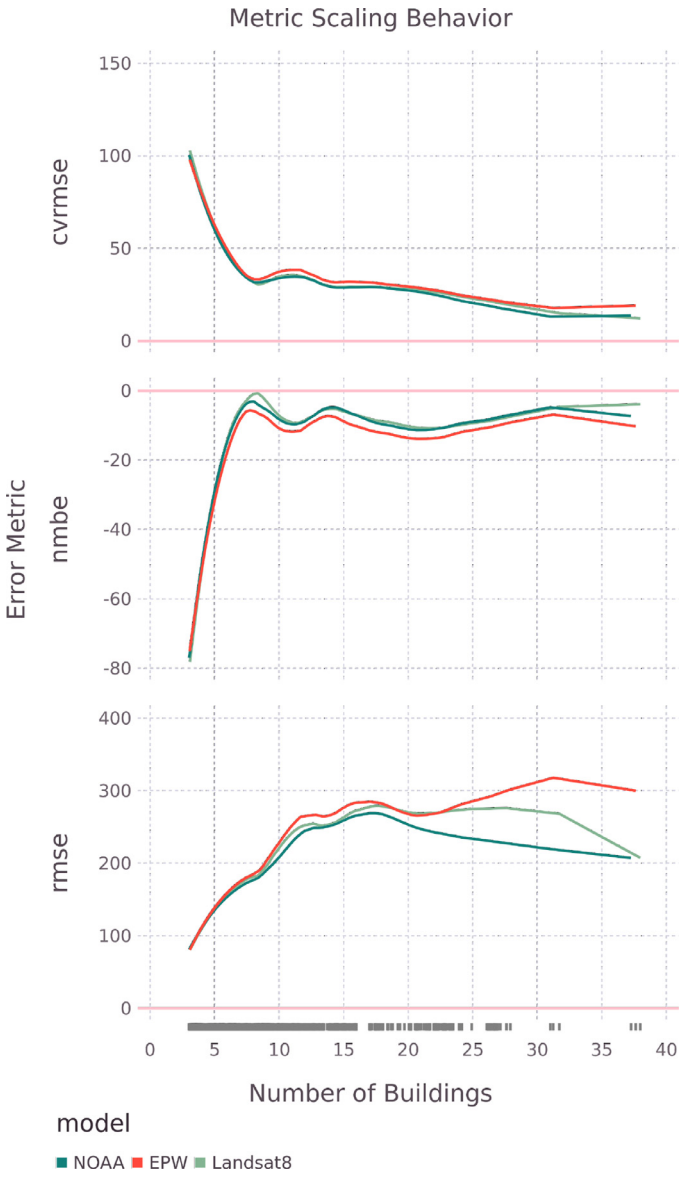

Fig. 8. Relationship between validation metrics and aggregation scales. Random noise was added to the number of buildings to give insight into the marginal distribution of buildings in each group.

Let us focus on a single variable like the extreme minimum values from the Shortwave Infrared 2 reflectance measurements, which captures light between wavelengths of 1.57μm and 1.65μm. To extend our intuition into the potential relationship between the Landsat measurements and electricity consumption, we now compute the shap value for every surface reflectance point within our test set. Doing so enables us to study how the variable is likely influencing the electricity consumption of the structure through its domain.

Fig. 10 sheds light on the potential utility of shortwave infrared measurements from Landsat8 for electricity prediction. In reading this plot, we see that a decrease of infrared surface reflectance to 0.0 is likely to intersect with the x axis at a shap value of about 0.05. As the shap values indicate the variables estimated impact on daily energy consumption in MWh, this would amount to an increase in the daily electricity consumption of the average structure by 50kWh per day. This represents a roughly a 3% increase to the baseline consumption of 1.78MWh. On the other side of this nonlinear curve, we see that higher values of infrared surface reflectance, like 0.3 are likely to correspond to a drop in electricity consumption. With a shap value of around −0.08, or an estimated

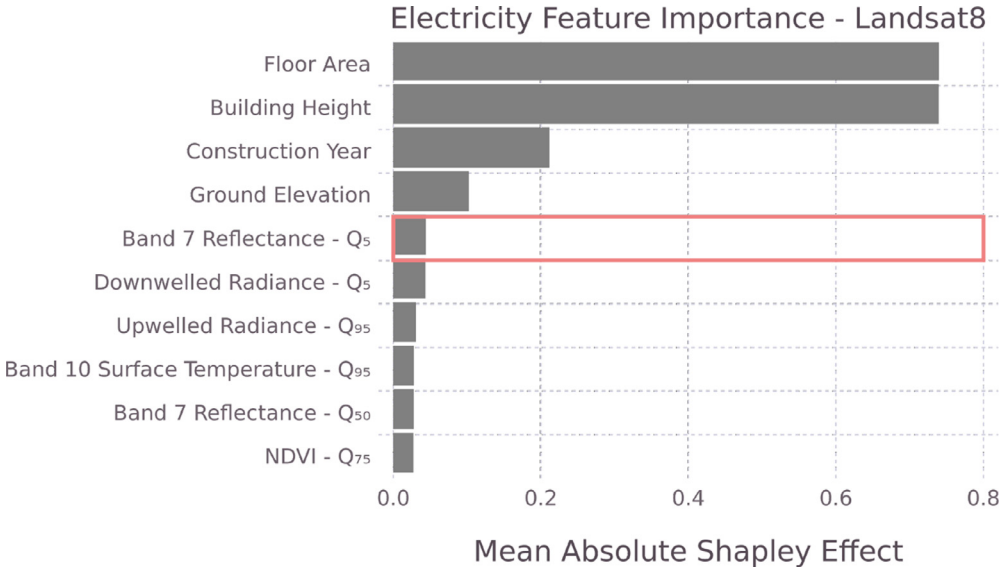

Fig. 9. $\mathbf{S}_3$ Feature Importance of Landsat8 value using the mean absolute shapely values.

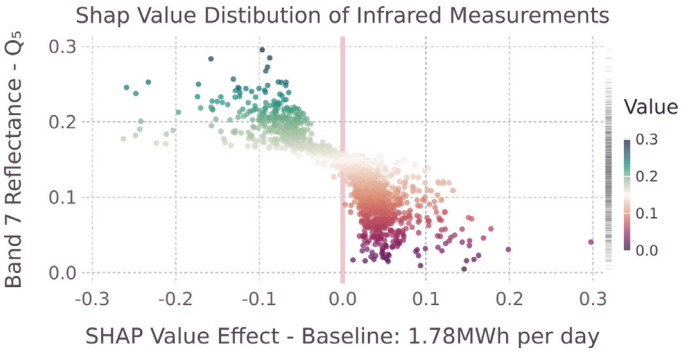

Fig. 10. A sample of SHAP values computed throughout the Shortwave Infrared 2 Surface Reflectance domain. Note: these are specific to electricity prediction in New York City and relative to a baseline prediction.

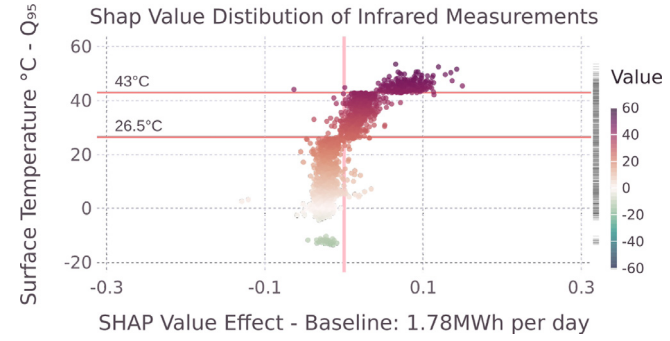

Fig. 11. $\mathbf{S}_3$ Shap values computed for Landsat8 Band 10 Surface Temperature measurements.

impact of −80kWh per day, for surface reflectance readings of 0.3, this would correspond to a decrease in electricity consumption of roughly 4–5%.

We can turn to a more intuitive metric from Landsat8, the land surface temperature, to understand how New York City's buildings respond to extreme heat. As New York City's buildings are almost entirely reliant on electricity for cooling, the relationship between the two is quite pronounced. Fig. 11 explores how extreme temperature readings, those in the 95th percentile of Landsat surface temperature readings at a location for the month, are likely to impact electricity consumption.

Notably, three distinct phases are seen. The first, below 25 °C, has no particular relationship with electricity consumption. A jump from the shap value of −0.02 to 0.01 is made as the temperature crosses the 26.5 °C (80°F) threshold, corresponding to an immediate 2% increase. In this second phase, we see a linear increase until we get to 43 °C (110°F), at which point a third phase is triggered with a shap value jump from 0.2 (20 kWh per day) to 0.7 (70 kWh per day). This corresponds to another overall increase in electricity consumption of roughly 3%, a total displacement of roughly 5–6% compared to the baseline scenario. This behavior profile reinforces the paradigm that energy required to meet cooling demands has a nonlinear relationship with temperature, particularly pronounced on sweltering days.

5.4.2. *Natural gas*

As NOAA provides the most substantial benefit for natural gas prediction, it is explored in detail in this section. As the NOAA data used within this analysis is averaged into the monthly interval, there is no difference between the schemas regarding added information. Therefore to reduce the complexity of the feature significance visualization, schema $\mathbf{S}_1$ is used, which only assumes the single value for each month.

The feature importance of each variable within the NOAA dataset can be found in Fig. 12. Surprisingly, the model's gas consumption prediction was more sensitive to temperature than the conditioned volume of the building. We can visualize the likely relationship between gas consumption and temperature in New York City by examining the shapely values through the domain of temperatures in New York City as seen in Fig. 13.

6. Discussion

Two datasets are particularly promising to improve the quality of energy predictions for large, cold cities like New York: NOAA's climate reanalysis and Landsat8. Landsat8 offers a 4-point improvement to CV(RMSE) for electricity prediction. NOAA offers the highest quality prediction for natural gas consumption, with a more marginal improvement of 1.3 points to CV(RMSE). Given that we utilized a statistical engine instead of a physics-based simulation, these are reasonable upper bounds to the added benefits.

The Landsat8 model benefited the most with the improved temporal resolution of schema $\mathbf{S}_3$. This is likely a result of Landsat8's high revisit frequency and dedicated onboard temperature sensor suite. Cloud obstructions are one of the primary sources of missing data, making the

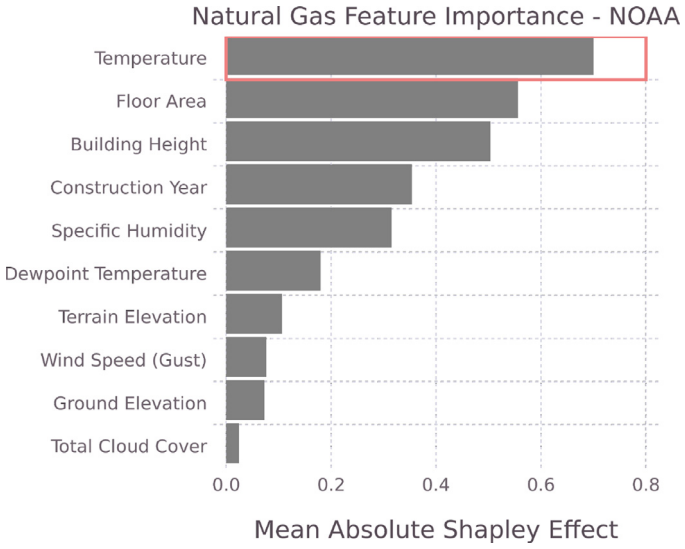

Fig. 12. NOAA Feature Importance - Natural Gas.

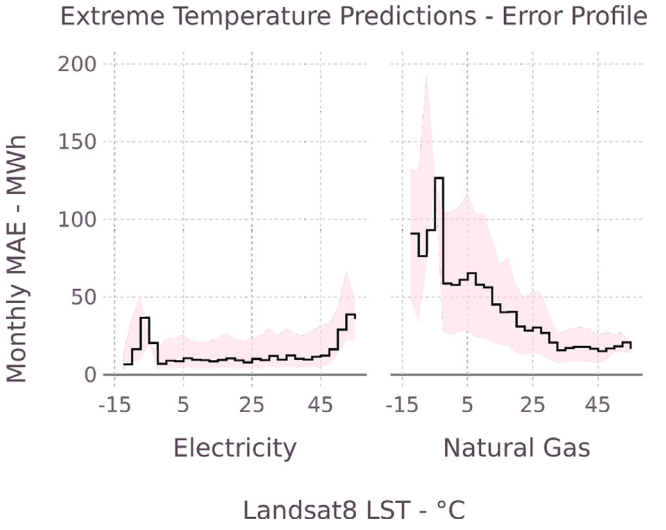

Fig. 14. MAE bucketed into temperature bins shows errors in estimation with extreme temperatures ($\mathbf{Q}_{95}$) from schema $\mathbf{S}_3$.

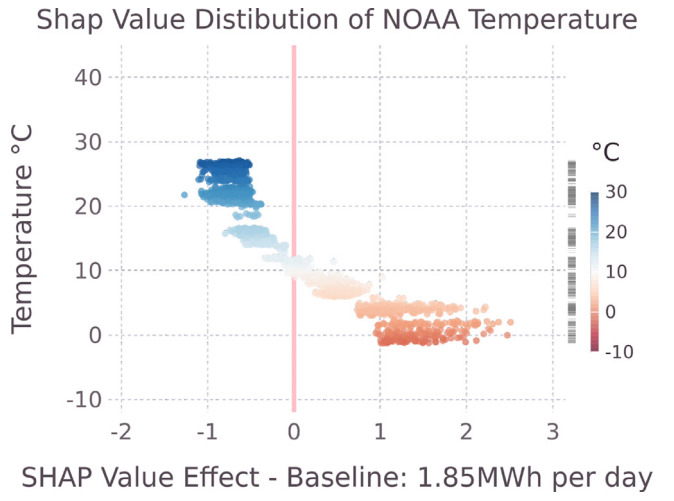

Fig. 13. $\mathbf{S}_1$ Shap values computed against NOAA RTMA temperature measurements.

redundancy of measurements each month more valuable for accurate prediction.

The improved resolution of temperature measurements possible due to Landsat8 enable us to examine extreme temperature events in the city and how the energy demands of the structures might respond in turn. The exponential response of electricity consumption with temperatures above 43 °C is an example of this new insight, with further inquiries into extreme temperatures likely continuing to be valuable with the acceleration of climate change. Extreme temperature effects on energy infrastructure may be particularly pertinent in dense urban areas such as New York City, which experiences high levels of urban heat island effect.

Figure 14 plots the predictive errors for the Landsat8 model against extreme temperature measurements. This figure highlights our capacity to accurately predict cooling demand response to temperatures below 45 °C with the assumption that high electricity consumption levels may serve as a surrogate for cooling demand in New York City.

The RMSE of the best performing schema, $\mathbf{s}_3$ found in Table B.21, shows that the CMIP dataset seems to provide a benefit which is at least as good as that of the EPW data. The other UBEM metrics seem to tell the same story, with similar and slightly lower CV(RMSE) and NMBE. This makes sense, as both datasets contain temperature data which is commonly recognized as the meteorological parameter most closely linked to energy consumption [41]. Likewise, with lower RMSE, CV(RMSE), and NMBE than EPW, this study serves as a promising indicator that CMIP may be a valuable resource for the prediction of building energy consumption through the lens of climate change. Assuming no significant retrofit modifications to the existing building stock, a statistical model like the one constructed in this study may be utilized for energy forecasting. To further extend the benefits of this work to explore retrofit scenarios, future research may also design a utility to conveniently link CMIP projections with simulation-based energy modeling for climate-aware retrofit analysis.

We recognize the potential benefits of more granular energy models, which may yield predictions specific to indoor air temperature or energy consumption of dwellings concerning their vertical displacement from the street [42]. While this research cannot provide similar benefits to high-resolution simulation-based models, the low RMSE of Sentinel-1's Synthetic Aperture Radar gives credence to the notion that remote sensing might be used to classify materials or surface roughness better [43,44]. Additionally, remote sensing and climate models might be used in a CFD-BES (Computational Fluid Dynamics and Building Energy System) study to enhance prediction quality and more easily design for new regions. A coupling of NOAA wind speed and Landsat8 land surface temperature measurements might provide boundary conditions for both wind and temperature, as required in the CFD-BES coupling of buildings in Tehran [9]. NASA's SRTM provides a rough elevation map of all points worldwide, providing valuable information for fluid simulations.

A lingering question exists as to why NOAA / CMIP temperature measurements were more significant for natural gas prediction than those collected from Landsat8. This performance gap in gas consumption prediction may be due to NOAA's awareness of minimum nighttime temperatures, whereas Landsat8's measurements are restricted between 3 PM and 4 PM. NOAA is likely to contain additional benefits for energy prediction, which was limited in this study. As the NOAA data was limited to a monthly resolution by Google Earth Engine's memory constraints, we imagine that expanded information in the full RTMA dataset may be more valuable. Further investigation of the synthesis of reanalysis data with energy modeling should be pursued to improve global coverage of buildings and enhance the spatial resolution of climate data.

Given that the entire dataset used is from New York City, which experiences one of the most significant urban heat island effects in the United States, we may be underestimating some local effects. The sig-

nificance of the urban heat island effect in increasing cooling demand and decreasing heating demand is likely understated in this study, potentially tucked into the bias of our model.

Finally, we note that many of our models used historically accurate recordings to make predictions, which is fundamentally different from the EPW files that always estimate weather. However, localized trends like those seen in 3 and 2 demonstrate a high consistency in the displacement of climate variables to EPW files. Thus future research seeking to generate hyperlocalized EPW files will likely capture most of the benefits presented in this work.

7. Conclusion

Microclimate data improves the quality of energy predictions in New York City across all metrics. The results of schema $\mathbf{S}_3$ B.21 may give us the most straightforward idea of potential benefits from each dataset. The schema $\mathbf{S}_3$ results indicate that Landsat8 may provide a nearly 4-point improvement in CV(RMSE) compared to the EPW model for individual building prediction. The natural gas model, which generally has a more challenging time accurately predicting consumption, may only appreciate a more modest benefit of 1.2 points to CV(RMSE). However, recent research highlights the potential of automating the process of collecting microclimate for use in building energy modeling [22]. Given this newfound capacity within microclimate modeling, the benefits of remote sensing may potentially be seen as “free money” to energy modelers.

We additionally explored the potential seasonal benefit of microclimate data, which is in the same spirit of research as other modern works in attempting to quantify the significance of microclimate in energy modeling [8]. We found that while Landsat8 provides benefit to electricity prediction consistently throughout the year, these benefits are particularly pronounced in the summer months as seen in Fig. 7, peaking with a nearly 10% improvement to EPW data in June. This study serves as validation that Landsat8’s thermal imaging suite may be a valuable tool to better understand cooling loads caused by UHI. The incorporation of NOAA’s RTMA is likely to provide predictive benefit for natural gas consumption in the winter and spring seasons of the northern hemisphere. The most significant improvements relative to EPW come between the months of Janurary and May in New York City, with a predictive improvement of roughly 3% during these months.

This study takes advantage of the relatively high quantity of monthly energy data from this three-year interval to additionally contextualize existing paradigms of aggregation prediction errors as laid out in [1]. Even small neighborhoods of buildings might appreciate most of the benefit of aggregation, making it easier to reach the accuracy compliance standards of ASHRAE Guideline 14.

A study area with more heterogenous climate scenarios and greater diversity of building distances from the nearest weather station will be required to conduct a more thorough investigation of EPW data quality. In addition, a more robust study of microclimate impact on traditional validation metrics like CV(RMSE), NMBE, and RMSE will require monthly and hourly disclosure of geolocated building energy consumption by more cities or countries. At the time of writing, New York City is the only city with a publicly available dataset at the temporal resolution of a month. The monthly interval is the highest resolution of time series data available, yet it also represents the lowest resolution at which UBEM validation metrics are defined. Without a larger pool of data from multiple cities, it will not be easy to test the robustness of urban energy models when applied to new locations on the planet.

Finally, this work serves as a validation study for the potential utility of CMIP data, which seems to have the same data quality as existing EPW files for energy prediction based on the RMSE scores of both models. By blending CMIP projections into simulation-based models, we may now have a viable path forward to estimate the effects of climate change on our urban energy demands.

The decarbonization of the built environment is one of the most difficult challenges in the effort to mitigate climate change. This work contextualizes the benefits of remote sensing and climate modeling for building energy modeling, helping us better understand the role of remote sensing in urban decarbonization. Perhaps as significant, the worldwide coverage of satellites makes it an attractive option to extend the benefits of building energy modeling to a global audience. This research represents a step forward in our capabilities and ability to link communities.

Data availability

All the environmental data was collected using Google Earth Engine, with the process outlined in [45]. The link to the GitHub repo with the tools required for convenient collection can be found here: https://github.com/trdougherty/tom.d. The reader may additionally find the source code, data, and intermediate processed results as the Zenodo repository: https://doi.org/10.5281/zenodo.7897689.

Declaration of Competing Interest

The authors declare that they have no known competing financial interests or personal relationships that could have appeared to influence the work reported in this paper

Acknowledgments

This material is based upon the work supported in part by the Stanford Sustainability Accelerator as part of the Data Commons project and the National Science Foundation under Grant No. 1941695. Any opinions, findings, and conclusions or recommendations expressed in this material are those of the author(s) and do not necessarily reflect the views of the National Science Foundation. Additionally, we would like to thank Stanford University and the Stanford Research Computing Center for providing computational resources and support that contributed to these research results.

Appendix A. Data summary

A1. Electricity data summary

Tables A.4, A.6 and A.7.

Table A.1
Electricity Data Summary: 1.

Model	Variable	Mean	Std. Dev	Min.	Q25	Median	Q75	Max.
-	Building Classification	nothing	nothing	Commercial	nothing	nothing	nothing	Residential
-	Daily Electricity (MWh)	1.83	2.755	0.1137	0.493	0.8841	1.848	24.46
-	Date	nothing	nothing	2018-01-01	2018-11-01	2019-08-01	2020-05-01	2020-12-01
-	Distance to Weather Station (km)	9.168	5.206	0.5509	5.061	8.411	12.42	24.15
-	Month	6.43	3.267	1	4	7	9	12
-	Property Id	$5.935 \cdot 10^{6}$	$3.071 \cdot 10^{6}$	7365	$3.072 \cdot 10^{6}$	$6.297 \cdot 10^{6}$	$6.794 \cdot 10^{6}$	16911026
-	Zipcode	$1.077 \cdot 10^{4}$	540.6	10,001	$1.031 \cdot 10^{4}$	$1.11 \cdot 10^{4}$	$1.123 \cdot 10^{4}$	11694
CMIP	Daily Maximum Temperature ($°C$)	19.14	8.787	4.541	10.93	20.23	27.74	32.15
CMIP	Daily Minimum Temperature (C)	9.629	8.221	−4.057	2.061	9.868	17.46	21.47
CMIP	Precipitation (kg $\cdot m^{-2} \cdot s^{-1}$)	$1.541 \cdot 10^{-5}$	$6.118 \cdot 10^{-6}$	$1.5 \cdot 10^{-6}$	$1.197 \cdot 10^{-5}$	$1.436 \cdot 10^{-5}$	$1.812 \cdot 10^{-5}$	$3.425 \cdot 10^{-5}$
Dynamic World	Coverage by Bare Land	0.05629	0.03267	0.02436	0.03981	0.04471	0.05586	0.3896
Dynamic World	Coverage by Built Environment	0.6635	0.137	0.02958	0.6732	0.7154	0.7295	0.7654
Dynamic World	Coverage by Crops	0.03201	0.005377	0.0192	0.02937	0.03169	0.0335	0.2454
Dynamic World	Coverage by Flooded Vegetation	0.03279	0.003448	0.01962	0.03073	0.03265	0.03479	0.09522
Dynamic World	Coverage by Grass	0.03026	0.005561	0.02123	0.02747	0.02923	0.03146	0.2987
Dynamic World	Coverage by Shrub	0.03818	0.02176	0.0213	0.02883	0.03088	0.0357	0.2397
Dynamic World	Coverage by Snow or Ice	0.04748	0.04746	0.0236	0.03245	0.03532	0.04018	0.4832
Dynamic World	Coverage by Trees	0.03904	0.02354	0.0229	0.0303	0.03316	0.03897	0.7473
Dynamic World	Coverage by Water	0.05553	0.03276	0.02409	0.03878	0.04468	0.05614	0.5136
Dynamic World	Likely Coverage Class	5.991	0.4073	0.6247	6	6	6	8
Null	Building Floor Area (m^2)	1385	1957	13.78	565.7	828.3	1496	$8.969 \cdot 10^{4}$
Null	Building Height (m)	79.61	66.46	0	46.73	64.24	81	1019
Null	Construction Year	1945	31.71	1706	1925	1931	1963	2022
Null	Ground Elevation (m)	52.81	37.16	−4	25	44	70	331
SAR	Incidence Angle from Ellipsoid (Deg.)	38.2	2.254	35.37	37.12	37.49	37.81	46.01
SAR	Vertical Transmis / Horizontal Receive (dB)	−8.885	4.193	−19.7	−12.1	−9.73	−6.705	9.692
SAR	Vertical Transmit / Vertical Receive (dB)	−1.321	3.383	−12.01	−3.899	−2.088	1.022	16.29
VIIRS	Average DNB Radiance ($nW \cdot cm^{-2} \cdot sr^{-1}$)	75.34	50.85	0	49.14	64.15	84.82	726.5
VIIRS	Number of Cloud-free Observations Used	10.63	2.659	0	8.897	10.51	13	19

Number of Buildings: 7782, Number of Data Points: 189,625

Table A.2
Electricity Data Summary: 2.

Model	Variable	Mean	Std. Dev	Min.	Q25	Median	Q75	Max.
Landsat8	Atmospheric Transmittance	0.7969	0.152	0.422	0.6992	0.8697	0.9312	0.9728
Landsat8	Blue	0.09598	0.03913	−0.1532	0.07445	0.09389	0.1154	0.9082
Landsat8	Downwelled Radiance ($W \cdot m^{-2} \cdot sr^{-1} \cdot \mu m^{-1}$)	0.7138	0.5583	0.061	0.223	0.451	1.131	1.974
Landsat8	Emissivity Standard Deviation	0.008015	0.002772	0	0.006345	0.007783	0.009504	0.03586
Landsat8	Emissivity of Band 10	0.9676	0.005805	0.9311	0.9644	0.9675	0.9701	0.9904
Landsat8	Green	0.1155	0.0421	−0.1616	0.09061	0.1132	0.1386	0.848
Landsat8	NDVI	0.06535	0.04642	−0.07266	0.0296	0.05593	0.09005	0.5599
Landsat8	Near Infrared	0.1696	0.06102	−0.05958	0.1301	0.1674	0.2107	0.8048
Landsat8	Pixel Distance to Cloud (km)	0.9878	1.158	0.01	0.1545	0.5773	1.377	12.47
Landsat8	Red	0.1227	0.0447	−0.1569	0.09607	0.1205	0.1474	0.8284
Landsat8	Shortwave Infrared 1	0.1658	0.0557	−0.006333	0.1336	0.1655	0.2014	0.6068
Landsat8	Shortwave Infrared 2	0.1396	0.04805	0.002208	0.1103	0.1383	0.1693	0.4804
Landsat8	Surface Temperature (°C)	22.94	14.83	−14.38	10.61	24.12	36.01	55.28
Landsat8	Surface Temperature Uncertainty (C)	4.314	1.223	1.893	3.326	4.101	5.466	7.64
Landsat8	Thermal Band Converted to Radiance ($W \cdot m^{-2} \cdot sr^{-1} \cdot \mu m^{-1}$)	8.356	1.502	4.633	7.084	8.605	9.643	11.86
Landsat8	Ultra Blue, Coastal Aerosol	0.08601	0.03716	−0.1921	0.06665	0.08402	0.1034	0.9147
Landsat8	Upwelled Radiance ($W \cdot m^{-2} \cdot sr^{-1} \cdot \mu m^{-1}$)	1.502	1.278	0.093	0.383	0.855	2.394	4.489
NOAA	Dewpoint Temperature (C)	7.571	8.703	−7.155	−0.5361	9.167	14.89	21.74
NOAA	Pressure (Pa)	$1.015 \cdot 10^5$	296.6	$1.004 \cdot 10^5$	$1.013 \cdot 10^5$	$1.015 \cdot 10^5$	$1.017 \cdot 10^5$	$1.022 \cdot 10^5$
NOAA	Specific Humidity (kg/kg)	0.007818	0.004044	0.002656	0.003946	0.007772	0.01086	0.01649
NOAA	Temperature (C)	13.98	8.54	−1.367	6.119	14.65	21.86	27.12
NOAA	Terrain Elevation (m)	17.92	12.97	0	8	16	27	89
NOAA	Total Cloud Cover (%)	45.66	8.447	28.12	38.21	47.21	52.39	63.41
NOAA	U-component Wind Speed (m/s)	0.6528	0.7238	−1.791	0.117	0.4897	1.242	3.624
NOAA	V-component Wind Speed (m/s)	−0.07602	0.5462	−3.19	−0.4717	−0.1012	0.2279	2.118
NOAA	Visability (m)	$1.479 \cdot 10^4$	570.8	$1.225 \cdot 10^4$	$1.435 \cdot 10^4$	$1.48 \cdot 10^4$	$1.532 \cdot 10^4$	$1.619 \cdot 10^4$
NOAA	Wind Direction (Deg.)	195	24.47	116.2	177.5	199.7	212	244.1
NOAA	Wind Speed (Gust) (m/s)	6.314	1.042	4.154	5.332	6.5	7.109	10.74
NOAA	Wind Speed (m/s)	3.007	0.6231	1.71	2.549	2.96	3.306	7.458
Sentinel-2	Aerosols	0.1814	0.01996	0.08526	0.1681	0.1806	0.1937	0.5017
Sentinel-2	Blue	0.1575	0.02361	0.08645	0.1421	0.1562	0.1718	0.3102
Sentinel-2	Green	0.1387	0.02811	0.06213	0.1201	0.1364	0.1564	0.3072
Sentinel-2	NDVI	0.07168	0.08379	−0.1966	0.01509	0.05667	0.1125	0.7589
Sentinel-2	Near Infrared	0.162	0.04612	0.0327	0.1306	0.16	0.1951	0.3585
Sentinel-2	Red	0.1375	0.03381	0.04306	0.1153	0.1351	0.1586	0.4719
Sentinel-2	Red Edge 1	0.1415	0.0343	0.04092	0.1197	0.1396	0.1631	0.481
Sentinel-2	Red Edge 2	0.1616	0.04325	0.03881	0.1324	0.1595	0.1921	0.6953
Sentinel-2	Red Edge 3	0.1724	0.04989	0.03698	0.1373	0.1688	0.2088	0.721
Sentinel-2	Red Edge 4	0.1775	0.05349	0.03305	0.1399	0.1738	0.2167	0.725
Sentinel-2	Shortwave Infrared 1	0.168	0.05076	0.01865	0.1357	0.1657	0.2015	0.4255
Sentinel-2	Shortwave Infrared 2	0.138	0.04368	0.01239	0.1099	0.1347	0.1653	0.4304
Sentinel-2	Water Vapor	0.05969	0.02122	0.0001865	0.04494	0.05769	0.07391	0.2833

Number of Buildings: 7782, Number of Data Points: 189,625

Table A.3
Electricity Data Summary: 3.

Model	Variable	Mean	Std. Dev	Min.	Q25	Median	Q75	Max.
EPW	Aerosol Optical Depth (thousandths) Daily Maxium	0.07226	0.08398	0	0	0	0.134	0.221
EPW	Aerosol Optical Depth (thousandths) Daily Median	0.07207	0.08382	0	0	0	0.133	0.221
EPW	Aerosol Optical Depth (thousandths) Daily Minimum	0.07187	0.08362	0	0	0	0.133	0.221
EPW	Albedo Daily Maxium	0.0671	0.07277	0	0	0	0.14	0.17
EPW	Albedo Daily Median	0.0671	0.07277	0	0	0	0.14	0.17
EPW	Albedo Daily Minimum	0.06686	0.07247	0	0	0	0.14	0.17
EPW	Atmospheric Station Pressure (Pa) Daily Maxium	1.02 e5	303.5	1.015 e5	1.018 e5	1.02 e5	1.023 e5	1.026 e5
EPW	Atmospheric Station Pressure (Pa) Daily Median	1.017 e5	304.4	1.005 e5	1.016 e5	1.016 e5	1.018 e5	1.024 e5
EPW	Atmospheric Station Pressure (Pa) Daily Minimum	1.013 e5	267.1	1.001 e5	1.012 e5	1.013 e5	1.015 e5	1.018 e5
EPW	Days Since Last Snowfall Daily Maxium	88	0	88	88	88	88	88
EPW	Days Since Last Snowfall Daily Median	88	0	88	88	88	88	88
EPW	Days Since Last Snowfall Daily Minimum	88	0	88	88	88	88	88
EPW	Dewpoint Temperature (°C) Daily Maxium	10.34	7.822	−3.3	2.8	8.6	17.5	22.2
EPW	Dewpoint Temperature (°C) Daily Median	6.861	8.653	−7.225	0	6.7	14.6	20
EPW	Dewpoint Temperature (°C) Daily Minimum	3.142	9.581	−14.7	−2.2	2.2	11.1	18.3
EPW	Diffuse Horizontal Illuminance (lux) Daily Maxium	3.27 e4	9694	1.692 e4	2.41 e4	2.945 e4	4.146 e4	4.861 e4
EPW	Diffuse Horizontal Illuminance (lux) Daily Median	3296	3512	0	0	1775	7222	1.07 e4
EPW	Diffuse Horizontal Illuminance (lux) Daily Minimum	0	0	0	0	0	0	0
EPW	Diffuse Horizontal Radiation (Wh/m^2) Daily Maxium	287.4	82.66	147	215.5	260	359	421
EPW	Diffuse Horizontal Radiation (Wh/m^2) Daily Median	28.61	30.12	0	0	13	56	90.5
EPW	Diffuse Horizontal Radiation (Wh/m^2) Daily Minimum	0	0	0	0	0	0	0
EPW	Direct Normal Illuminance (lux) Daily Maxium	5.335 e4	1.376 e4	126	4.353 e4	5.162 e4	6.77 e4	7.15 e4
EPW	Direct Normal Illuminance (lux) Daily Median	474.9	784.2	0	0	0	606	3050
EPW	Direct Normal Illuminance (lux) Daily Minimum	0	0	0	0	0	0	0
EPW	Direct Normal Radiation (Wh/m^2) Daily Maxium	639.6	94.42	2	608	658	689	745
EPW	Direct Normal Radiation (Wh/m^2) Daily Median	11.7	18.44	0	0	2.75	14.5	79
EPW	Direct Normal Radiation (Wh/m^2) Daily Minimum	0	0	0	0	0	0	0
EPW	Drybulb Temperature (°C) Daily Maxium	17.82	8.771	2.2	11.1	16.7	26.1	31.1
EPW	Drybulb Temperature (°C) Daily Median	14.21	8.274	−1.7	8.3	13.05	22.65	26.4
EPW	Drybulb Temperature (°C) Daily Minimum	10.55	8.081	−4.4	4.4	10	18.3	22.8
EPW	Extraterrestrial Direct Normal Radiation (Wh/m^2) Daily Maxium	1364	31.96	1322	1332	1358	1398	1414
EPW	Extraterrestrial Direct Normal Radiation (Wh/m^2) Daily Median	723.5	558	0	93.5	923.8	1322	1336
EPW	Extraterrestrial Direct Normal Radiation (Wh/m^2) Daily Minimum	0	0	0	0	0	0	0
EPW	Extraterrestrial Horizontal Radiation (Wh/m^2) Daily Maxium	1008	215.6	612	825	1056	1234	1253
EPW	Extraterrestrial Horizontal Radiation (Wh/m^2) Daily Median	129.2	132.3	0	1.75	74.75	287.5	343
EPW	Extraterrestrial Horizontal Radiation (Wh/m^2) Daily Minimum	0	0	0	0	0	0	0
EPW	Global Horizontal Illuminance (lux) Daily Maxium	7.485 e4	2.186 e4	1.684 e4	6.077 e4	7.936 e4	9.47 e4	1.049 e5
EPW	Global Horizontal Illuminance (lux) Daily Median	4366	4700	0	0	2100	8950	1.243 e4
EPW	Global Horizontal Illuminance (lux) Daily Minimum	0	0	0	0	0	0	0

Number of Buildings: 7782, Number of Data Points: 189,625

Table A.4
Electricity Data Summary: 4.

Model	Variable	Mean	Std. Dev	Min.	Q25	Median	Q75	Max.
EPW	Global Horizontal Radiation (Wh/m^2) Daily Maxium	670.8	188.8	147	518.5	697.5	831	895.5
EPW	Global Horizontal Radiation (Wh/m^2) Daily Median	40.09	42.64	0	0	19.5	80.5	113.5
EPW	Global Horizontal Radiation (Wh/m^2) Daily Minimum	0	0	0	0	0	0	0
EPW	Horizontal Infrared Radiation Intensity (Wh/m^2) Daily Maxium	365	48.46	288	320	355.5	416	448
EPW	Horizontal Infrared Radiation Intensity (Wh/m^2) Daily Median	338.2	46.23	257	301.5	329	381.8	417.5
EPW	Horizontal Infrared Radiation Intensity (Wh/m^2) Daily Minimum	307.5	43.61	231	274	305	347	380
EPW	Liquid Precipitation Depth (mm) Daily Maxium	0	0	0	0	0	0	0
EPW	Liquid Precipitation Depth (mm) Daily Median	0	0	0	0	0	0	0
EPW	Liquid Precipitation Depth (mm) Daily Minimum	0	0	0	0	0	0	0
EPW	Liquid Precipitation Quantity (hr) Daily Maxium	1	0	1	1	1	1	1
EPW	Liquid Precipitation Quantity (hr) Daily Median	1	0	1	1	1	1	1
EPW	Liquid Precipitation Quantity (hr) Daily Minimum	1	0	1	1	1	1	1
EPW	Opaque Sky Cover Daily Maxium	9.81	0.4646	8	10	10	10	10
EPW	Opaque Sky Cover Daily Median	4.787	1.376	3	3.75	4.75	5.5	10
EPW	Opaque Sky Cover Daily Minimum	0.05576	0.3274	0	0	0	0	3
EPW	Precipitable Water (mm) Daily Maxium	118.5	124.4	9	18.5	37	194.5	400
EPW	Precipitable Water (mm) Daily Median	102.5	111.3	7	15.25	33.5	170	390
EPW	Precipitable Water (mm) Daily Minimum	87.15	100.4	5	12	28	129	379
EPW	Relative Humidity Daily Maxium	82.51	7.217	60	79	83	88.5	100
EPW	Relative Humidity Daily Median	61.44	7.404	46.5	57	61	65.75	96
EPW	Relative Humidity Daily Minimum	43.7	6.565	31	39	44	49	58
EPW	Snow Depth (cm) Daily Maxium	0	0	0	0	0	0	0
EPW	Snow Depth (cm) Daily Median	0	0	0	0	0	0	0
EPW	Snow Depth (cm) Daily Minimum	0	0	0	0	0	0	0
EPW	Total Sky Cover Daily Maxium	10	0	10	10	10	10	10
EPW	Total Sky Cover Daily Median	6.474	1.463	3	5.5	7	7.5	10
EPW	Total Sky Cover Daily Minimum	0.1337	0.4263	0	0	0	0	3
EPW	Visibility (km) Daily Maxium	25.79	5.873	16	24	24.1	32	32.2
EPW	Visibility (km) Daily Median	18.45	4.116	3.2	16	19.3	21.6	24.1
EPW	Visibility (km) Daily Minimum	11.82	3.626	0.8	8	12.8	14.4	16.8
EPW	Wind Direction (deg) Daily Maxium	324.3	16.73	300	310	320	340	360
EPW	Wind Direction (deg) Daily Median	203.6	39.26	50	180	200	230	275
EPW	Wind Direction (deg) Daily Minimum	46.47	49.47	10	20	20	40	220
EPW	Wind Speed (m/s) Daily Maxium	8.239	1.209	5.95	7.2	8.2	9.05	10.8
EPW	Wind Speed (m/s) Daily Median	5.22	0.902	3.6	4.6	4.9	5.8	7.7
EPW	Wind Speed (m/s) Daily Minimum	2.368	0.6251	1.5	2.1	2.6	2.6	5.2
EPW	Zenith Luminance (Cd/m^2) Daily Maxium	7414	1395	4160	6522	7610	8434	9980
EPW	Zenith Luminance (Cd/m^2) Daily Median	792.4	876.7	0	0	474.2	1278	2701
EPW	Zenith Luminance (Cd/m^2) Daily Minimum	0	0	0	0	0	0	0

Number of Buildings: 7782, Number of Data Points: 189,625

Table A.5
Natural Gas Data Summary: 1.

Model	Variable	Mean	Std. Dev	Min.	Q25	Median	Q75	Max.
-	Building Classification	nothing	nothing	Commercial	nothing	nothing	nothing	Residential
-	Daily Natural Gas (MWh)	2.504	3.547	0.002838	0.2737	1.21	3.273	30.74
-	Date	nothing	nothing	2018-01-01	2018-12-01	2019-08-01	2020-05-01	2020-12-01
-	Distance to Weather Station (km)	9.238	5.201	0.5509	5.166	8.463	12.48	24.15
-	Month	6.413	3.282	1	4	6	9	12
-	Property Id	$5.921 \cdot 10^{6}$	$3.083 \cdot 10^{6}$	8604	$2.977 \cdot 10^{6}$	$6.297 \cdot 10^{6}$	$6.794 \cdot 10^{6}$	16911026
-	Zipcode	$1.077 \cdot 10^{4}$	534.8	10,001	$1.045 \cdot 10^{4}$	$1.11 \cdot 10^{4}$	$1.123 \cdot 10^{4}$	11694
CMIP	Daily Maximum Temperature (°C)	19.03	8.774	4.541	10.88	20.22	27.3	32.15
CMIP	Daily Minimum Temperature (C)	9.517	8.204	−4.057	2.061	9.868	17.39	21.47
CMIP	Precipitation (kg $\cdot m^{-2} \cdot s^{-1}$)	$1.538 \cdot 10^{-5}$	$6.086 \cdot 10^{-6}$	$1.5 \cdot 10^{-6}$	$1.197 \cdot 10^{-5}$	$1.436 \cdot 10^{-5}$	$1.812 \cdot 10^{-5}$	$3.425 \cdot 10^{-5}$
Dynamic World	Coverage by Bare Land	0.05523	0.03133	0.02436	0.03966	0.04444	0.05495	0.3896
Dynamic World	Coverage by Built Environment	0.6679	0.1292	0.0316	0.6758	0.7158	0.7296	0.7654
Dynamic World	Coverage by Crops	0.03207	0.005401	0.0192	0.02947	0.03174	0.03354	0.2454
Dynamic World	Coverage by Flooded Vegetation	0.03277	0.003425	0.01962	0.03074	0.03265	0.03476	0.08482
Dynamic World	Coverage by Grass	0.03026	0.005587	0.02123	0.02749	0.02923	0.03143	0.2987
Dynamic World	Coverage by Shrub	0.03756	0.02044	0.02251	0.02885	0.03088	0.03549	0.2397
Dynamic World	Coverage by Snow or Ice	0.04584	0.04318	0.0236	0.03243	0.03527	0.04	0.4828
Dynamic World	Coverage by Trees	0.03908	0.0237	0.0229	0.03032	0.03317	0.03887	0.7195
Dynamic World	Coverage by Water	0.05455	0.03152	0.02409	0.03867	0.04447	0.0553	0.5136
Dynamic World	Likely Coverage Class	5.984	0.3869	0.9036	6	6	6	8
Null	Building Floor Area (m^2)	1382	1985	13.78	562.6	819.6	1483	$8.969 \cdot 10^{4}$
Null	Building Height (m)	76.95	60.04	0	47	64.14	79.74	1019
Null	Construction Year	1945	31.52	1706	1925	1931	1962	2022
Null	Ground Elevation (m)	53.55	37.97	−4	25	44	72	331
SAR	Incidence Angle from Ellipsoid (Deg.)	38.18	2.222	35.37	37.14	37.5	37.81	46.01
SAR	Vertical Transmis / Horizontal Receive (dB)	−9.069	4.022	−19.7	−12.14	−9.814	−7.049	9.692
SAR	Vertical Transmit / Vertical Receive (dB)	−1.467	3.3	−12.01	−3.949	−2.238	0.7958	15.59
VIIRS	Average DNB Radiance ($nW \cdot cm^{-2} \cdot sr^{-1}$)	73.24	47.43	0	48.84	63.45	83.4	711.6
VIIRS	Number of Cloud-free Observations Used	10.64	2.641	0	8.978	10.53	13	19

Number of Buildings: 7229, Number of Data Points: 172,213

Table A.6
Natural Gas Data Summary: 2.

Model	Variable	Mean	Std. Dev	Min.	Q25	Median	Q75	Max.
Landsat8	Atmospheric Transmittance	0.7988	0.151	0.422	0.6998	0.8704	0.9313	0.9728
Landsat8	Blue	0.09622	0.03908	−0.1532	0.0747	0.09395	0.1155	0.9082
Landsat8	Downwelled Radiance ($W \cdot m^{-2} \cdot sr^{-1} \cdot \mu m^{-1}$)	0.7063	0.5547	0.061	0.223	0.45	1.127	1.974
Landsat8	Emissivity Standard Deviation	0.008029	0.002719	0	0.00637	0.007785	0.009494	0.03586
Landsat8	Emissivity of Band 10	0.9676	0.005671	0.9311	0.9644	0.9675	0.9701	0.9904
Landsat8	Green	0.1158	0.04195	−0.1616	0.09095	0.1133	0.1387	0.848
Landsat8	NDVI	0.06635	0.04675	−0.07266	0.03027	0.05711	0.09115	0.5599
Landsat8	Near Infrared	0.1707	0.06057	−0.05958	0.131	0.1683	0.2115	0.8048
Landsat8	Pixel Distance to Cloud (km)	0.991	1.163	0.01	0.1551	0.5767	1.381	12.47
Landsat8	Red	0.1231	0.04451	−0.1569	0.09644	0.1206	0.1475	0.8284
Landsat8	Shortwave Infrared 1	0.1667	0.05514	−0.006333	0.1347	0.166	0.2019	0.6068
Landsat8	Shortwave Infrared 2	0.1404	0.0477	0.002208	0.1112	0.1388	0.1697	0.4804
Landsat8	Surface Temperature (°C)	22.78	14.78	−14.38	10.45	23.94	35.75	55.28
Landsat8	Surface Temperature Uncertainty (C)	4.31	1.221	1.893	3.324	4.097	5.461	7.64
Landsat8	Thermal Band Converted to Radiance ($W \cdot m^{-2} \cdot sr^{-1} \cdot \mu m^{-1}$)	8.341	1.497	4.633	7.068	8.584	9.629	11.86
Landsat8	Ultra Blue, Coastal Aerosol	0.0862	0.03715	−0.1921	0.06683	0.08406	0.1034	0.9147
Landsat8	Upwelled Radiance ($W \cdot m^{-2} \cdot sr^{-1} \cdot \mu m^{-1}$)	1.484	1.269	0.093	0.383	0.853	2.385	4.489
NOAA	Dewpoint Temperature (C)	7.445	8.669	−7.155	−0.5827	9.063	14.83	21.74
NOAA	Pressure (Pa)	$1.015 \cdot 10^5$	297.1	$1.004 \cdot 10^5$	$1.013 \cdot 10^5$	$1.015 \cdot 10^5$	$1.017 \cdot 10^5$	$1.022 \cdot 10^5$
NOAA	Specific Humidity (kg/kg)	0.007752	0.004021	0.002656	0.003929	0.00775	0.01085	0.01649
NOAA	Temperature (C)	13.86	8.511	−1.367	6.078	14.58	21.78	27.12
NOAA	Terrain Elevation (m)	17.96	13.01	0	8	16	27	89
NOAA	Total Cloud Cover (%)	45.66	8.411	28.12	38.24	47.31	52.37	63.41
NOAA	U-component Wind Speed (m/s)	0.6603	0.7206	−1.791	0.1302	0.4937	1.248	3.624
NOAA	V-component Wind Speed (m/s)	−0.08125	0.5402	−3.19	−0.4722	−0.1056	0.2211	2.118
NOAA	Visability (m)	$1.479 \cdot 10^4$	571.8	$1.225 \cdot 10^4$	$1.434 \cdot 10^4$	$1.48 \cdot 10^4$	$1.531 \cdot 10^4$	$1.619 \cdot 10^4$
NOAA	Wind Direction (Deg.)	195.2	24.34	116.2	177.6	199.8	212.1	244.1
NOAA	Wind Speed (Gust) (m/s)	6.325	1.039	4.154	5.349	6.52	7.116	10.74
NOAA	Wind Speed (m/s)	3.014	0.6236	1.71	2.558	2.967	3.312	7.458
Sentinel-2	Aerosols	0.1816	0.01979	0.08526	0.1684	0.1807	0.1938	0.5017
Sentinel-2	Blue	0.1578	0.02339	0.09001	0.1424	0.1563	0.1718	0.3102
Sentinel-2	Green	0.139	0.02783	0.06213	0.1204	0.1365	0.1565	0.3072
Sentinel-2	NDVI	0.0741	0.08397	−0.1966	0.01677	0.05891	0.1146	0.7119
Sentinel-2	Near Infrared	0.163	0.04555	0.0327	0.1315	0.1607	0.1958	0.3585
Sentinel-2	Red	0.1379	0.03351	0.04438	0.1156	0.1352	0.1587	0.4719
Sentinel-2	Red Edge 1	0.142	0.03389	0.04092	0.1202	0.1398	0.1633	0.481
Sentinel-2	Red Edge 2	0.1624	0.04271	0.03881	0.1332	0.16	0.1927	0.6953
Sentinel-2	Red Edge 3	0.1733	0.04934	0.03698	0.1381	0.1694	0.2094	0.721
Sentinel-2	Red Edge 4	0.1785	0.0529	0.03305	0.1408	0.1746	0.2175	0.725
Sentinel-2	Shortwave Infrared 1	0.1689	0.05009	0.01865	0.1366	0.1662	0.2019	0.4255
Sentinel-2	Shortwave Infrared 2	0.1388	0.04326	0.01239	0.1107	0.1352	0.1658	0.4304
Sentinel-2	Water Vapor	0.06035	0.02102	0.0001865	0.0459	0.05822	0.07451	0.2833

Number of Buildings: 7229, Number of Data Points: 172,213

Table A.7
Natural Gas Data Summary: 3.

Model	Variable	Mean	Std. Dev	Min.	Q25	Median	Q75	Max.
EPW	Aerosol Optical Depth (thousandths) Daily Maxium	0.07481	0.08418	0	0	0	0.134	0.221
EPW	Aerosol Optical Depth (thousandths) Daily Median	0.07461	0.08402	0	0	0	0.133	0.221
EPW	Aerosol Optical Depth (thousandths) Daily Minimum	0.0744	0.08381	0	0	0	0.133	0.221
EPW	Albedo Daily Maxium	0.06965	0.07296	0	0	0	0.14	0.17
EPW	Albedo Daily Median	0.06965	0.07296	0	0	0	0.14	0.17
EPW	Albedo Daily Minimum	0.06939	0.07265	0	0	0	0.14	0.17
EPW	Atmospheric Station Pressure (Pa) Daily Maxium	1.021 e5	302.4	1.015 e5	1.018 e5	1.02 e5	1.023 e5	1.026 e5
EPW	Atmospheric Station Pressure (Pa) Daily Median	1.017 e5	305.7	1.005 e5	1.016 e5	1.016 e5	1.018 e5	1.024 e5
EPW	Atmospheric Station Pressure (Pa) Daily Minimum	1.013 e5	269	1.001 e5	1.012 e5	1.013 e5	1.015 e5	1.018 e5
EPW	Days Since Last Snowfall Daily Maxium	88	0	88	88	88	88	88
EPW	Days Since Last Snowfall Daily Median	88	0	88	88	88	88	88
EPW	Days Since Last Snowfall Daily Minimum	88	0	88	88	88	88	88
EPW	Dewpoint Temperature (°C) Daily Maxium	10.24	7.801	−3.3	2.8	8.6	17.5	22.2
EPW	Dewpoint Temperature (°C) Daily Median	6.743	8.631	−7.225	0	6.35	14.6	20
EPW	Dewpoint Temperature (°C) Daily Minimum	3.019	9.557	−14.7	−2.2	2.2	11.1	18.3
EPW	Diffuse Horizontal Illuminance (lux) Daily Maxium	3.25 e4	9656	1.692 e4	2.41 e4	2.945 e4	4.146 e4	4.861 e4
EPW	Diffuse Horizontal Illuminance (lux) Daily Median	3269	3514	0	0	1775	7222	1.07 e4
EPW	Diffuse Horizontal Illuminance (lux) Daily Minimum	0	0	0	0	0	0	0
EPW	Diffuse Horizontal Radiation (Wh/m^2) Daily Maxium	285.8	82.41	147	215.5	260	359	421
EPW	Diffuse Horizontal Radiation (Wh/m^2) Daily Median	28.32	30.09	0	0	13	56	90.5
EPW	Diffuse Horizontal Radiation (Wh/m^2) Daily Minimum	0	0	0	0	0	0	0
EPW	Direct Normal Illuminance (lux) Daily Maxium	5.373 e4	1.38 e4	126	4.373 e4	5.389 e4	6.77 e4	7.15 e4
EPW	Direct Normal Illuminance (lux) Daily Median	474.2	784.7	0	0	0	606	3050
EPW	Direct Normal Illuminance (lux) Daily Minimum	0	0	0	0	0	0	0
EPW	Direct Normal Radiation (Wh/m^2) Daily Maxium	639.8	94.65	2	608	661	689	745
EPW	Direct Normal Radiation (Wh/m^2) Daily Median	11.38	17.99	0	0	2.75	14.5	79
EPW	Direct Normal Radiation (Wh/m^2) Daily Minimum	0	0	0	0	0	0	0
EPW	Drybulb Temperature (°C) Daily Maxium	17.74	8.758	2.2	11.1	16.7	26.1	31.1
EPW	Drybulb Temperature (°C) Daily Median	14.12	8.25	−1.7	8.3	13.05	22.65	26.4
EPW	Drybulb Temperature (°C) Daily Minimum	10.46	8.061	−4.4	4.4	10	18.3	22.8
EPW	Extraterrestrial Direct Normal Radiation (Wh/m^2) Daily Maxium	1364	31.93	1322	1332	1358	1398	1414
EPW	Extraterrestrial Direct Normal Radiation (Wh/m^2) Daily Median	718	558.5	0	93.5	923.8	1322	1336
EPW	Extraterrestrial Direct Normal Radiation (Wh/m^2) Daily Minimum	0	0	0	0	0	0	0
EPW	Extraterrestrial Horizontal Radiation (Wh/m^2) Daily Maxium	1006	215.8	612	825	1056	1234	1253
EPW	Extraterrestrial Horizontal Radiation (Wh/m^2) Daily Median	128	132.2	0	1.75	74.75	287.5	343
EPW	Extraterrestrial Horizontal Radiation (Wh/m^2) Daily Minimum	0	0	0	0	0	0	0
EPW	Global Horizontal Illuminance (lux) Daily Maxium	7.454 e4	2.182 e4	1.684 e4	6.077 e4	7.936 e4	9.47 e4	1.049 e5
EPW	Global Horizontal Illuminance (lux) Daily Median	4313	4682	0	0	2100	8950	1.243 e4
EPW	Global Horizontal Illuminance (lux) Daily Minimum	0	0	0	0	0	0	0

Number of Buildings: 7229, Number of Data Points: 172,213

A2. Natural gas data summary

Table A.8

Table A.8
Natural Gas Data Summary: 4.

Model	Variable	Mean	Std. Dev	Min.	Q25	Median	Q75	Max.
EPW	Global Horizontal Radiation (Wh/m^2) Daily Maxium	670.8	188.8	147	518.5	697.5	831	895.5
EPW	Global Horizontal Radiation (Wh/m^2) Daily Median	40.09	42.64	0	0	19.5	80.5	113.5
EPW	Global Horizontal Radiation (Wh/m^2) Daily Minimum	0	0	0	0	0	0	0
EPW	Horizontal Infrared Radiation Intensity (Wh/m^2) Daily Maxium	365	48.46	288	320	355.5	416	448
EPW	Horizontal Infrared Radiation Intensity (Wh/m^2) Daily Median	338.2	46.23	257	301.5	329	381.8	417.5
EPW	Horizontal Infrared Radiation Intensity (Wh/m^2) Daily Minimum	307.5	43.61	231	274	305	347	380
EPW	Liquid Precipitation Depth (mm) Daily Maxium	0	0	0	0	0	0	0
EPW	Liquid Precipitation Depth (mm) Daily Median	0	0	0	0	0	0	0
EPW	Liquid Precipitation Depth (mm) Daily Minimum	0	0	0	0	0	0	0
EPW	Liquid Precipitation Quantity (hr) Daily Maxium	1	0	1	1	1	1	1
EPW	Liquid Precipitation Quantity (hr) Daily Median	1	0	1	1	1	1	1
EPW	Liquid Precipitation Quantity (hr) Daily Minimum	1	0	1	1	1	1	1
EPW	Opaque Sky Cover Daily Maxium	9.81	0.4646	8	10	10	10	10
EPW	Opaque Sky Cover Daily Median	4.787	1.376	3	3.75	4.75	5.5	10
EPW	Opaque Sky Cover Daily Minimum	0.05576	0.3274	0	0	0	0	3
EPW	Precipitable Water (mm) Daily Maxium	118.5	124.4	9	18.5	37	194.5	400
EPW	Precipitable Water (mm) Daily Median	102.5	111.3	7	15.25	33.5	170	390
EPW	Precipitable Water (mm) Daily Minimum	87.15	100.4	5	12	28	129	379
EPW	Relative Humidity Daily Maxium	82.51	7.217	60	79	83	88.5	100
EPW	Relative Humidity Daily Median	61.44	7.404	46.5	57	61	65.75	96
EPW	Relative Humidity Daily Minimum	43.7	6.565	31	39	44	49	58
EPW	Snow Depth (cm) Daily Maxium	0	0	0	0	0	0	0
EPW	Snow Depth (cm) Daily Median	0	0	0	0	0	0	0
EPW	Snow Depth (cm) Daily Minimum	0	0	0	0	0	0	0
EPW	Total Sky Cover Daily Maxium	10	0	10	10	10	10	10
EPW	Total Sky Cover Daily Median	6.474	1.463	3	5.5	7	7.5	10
EPW	Total Sky Cover Daily Minimum	0.1337	0.4263	0	0	0	0	3
EPW	Visibility (km) Daily Maxium	25.79	5.873	16	24	24.1	32	32.2
EPW	Visibility (km) Daily Median	18.45	4.116	3.2	16	19.3	21.6	24.1
EPW	Visibility (km) Daily Minimum	11.82	3.626	0.8	8	12.8	14.4	16.8
EPW	Wind Direction (deg) Daily Maxium	324.3	16.73	300	310	320	340	360
EPW	Wind Direction (deg) Daily Median	203.6	39.26	50	180	200	230	275
EPW	Wind Direction (deg) Daily Minimum	46.47	49.47	10	20	20	40	220
EPW	Wind Speed (m/s) Daily Maxium	8.239	1.209	5.95	7.2	8.2	9.05	10.8
EPW	Wind Speed (m/s) Daily Median	5.22	0.902	3.6	4.6	4.9	5.8	7.7
EPW	Wind Speed (m/s) Daily Minimum	2.368	0.6251	1.5	2.1	2.6	2.6	5.2
EPW	Zenith Luminance (Cd/m^2) Daily Maxium	7414	1395	4160	6522	7610	8434	9980
EPW	Zenith Luminance (Cd/m^2) Daily Median	792.4	876.7	0	0	474.2	1278	2701
EPW	Zenith Luminance (Cd/m^2) Daily Minimum	0	0	0	0	0	0	0

Number of Buildings: 7229, Number of Data Points: 172,213

Appendix B. Results

B1. Monthly MAE results

Tables B.1-B.8

Table B.1
Individual Monthly Building MAE for Schema $\mathbf{S}_1$ - Commercial Electricity.

Model	1	2	3	4	5	6	7	8	9	10	11	12
Null	40.1	36.8	35.1	35.2	40.6	41.5	47.9	46.1	42.6	39.4	36.5	36.3
NOAA	40.4	36.5	34.8	35	40	41.3	47.2	45	42.1	39.8	36.4	36.2
CMIP	40.8	37	35.2	35.4	40.7	41.7	47.4	45.3	43.2	40.1	37	36.5
EPW	40.8	36.9	35.3	35.7	40.6	42.5	48.4	46.5	43.2	40.5	37.1	36.6
Landsat8	41	36.9	34.7	34.3	38.6	40.8	46.3	45.1	41.7	39.2	36.5	36.3
VIIRS	39.4	35.9	35.5	34.9	39.4	39.7	46.3	45.3	41	38.7	37	38.7
SAR	39.7	36.3	34.8	34.9	40.2	40.3	46.5	45.1	41.5	38.2	35.8	36.1
Dynamic World	40.6	36.5	34.2	33.7	39.4	41.2	47.4	45.7	41.9	38.1	36.3	37.6
Sentinel-2	40.3	36.2	34.1	34	39.1	41	46.6	45.4	42.2	38.8	36.6	36.5

Table B.2
Individual Monthly Building MAE for Schema $\mathbf{S}_1$ - Manufacturing Electricity.

Model	1	2	3	4	5	6	7	8	9	10	11	12
Null	40.2	36.6	43.2	39.9	43	42.1	42.2	43	41.8	42.4	41.2	42.4
NOAA	38.8	34.3	40.1	36.2	39.2	45	47.8	48	43.8	39.4	36.8	37.8
CMIP	37.9	34.1	38.9	35.9	39.5	45.5	49	49.1	43.4	39	37.1	38.2
EPW	39.5	35.1	40.9	37.5	40.1	46.3	47.9	48.3	43.5	41	37.8	39
Landsat8	37.8	32.1	37.9	33.3	38.8	42.2	45.6	45.1	44.2	38.1	36.8	36.8
VIIRS	41.7	36.5	43.5	40.5	42.6	44.1	43.8	43.6	41.4	43.2	42.1	42.8
SAR	40.4	35.7	41.9	39	42.7	42.6	42.4	42.9	42	42	40	40.6
Dynamic World	41.9	36.1	41.9	37.2	41.1	41	42.3	42.7	41	42.2	40.4	43
Sentinel-2	39.2	33.2	38.3	34.1	38.6	41.4	45.9	45.5	43.1	42.7	40.7	40.6

Table B.3
Individual Monthly Building MAE for Schema $\mathbf{S}_1$ - Residential Electricity.

Model	1	2	3	4	5	6	7	8	9	10	11	12
Null	16.7	18	17.9	17.7	18.6	16.1	19	16.9	16.7	18.9	18	16.8
NOAA	15.6	16.5	15.7	15	16.4	17	19.2	17.7	17.5	16.7	15.2	13.7
CMIP	16.1	17.3	16.3	16.1	17.8	18.1	20.2	18.4	18.1	17.8	16.3	15.2
EPW	15.7	16.9	16	15.9	16.9	17.3	19.2	17.5	17.5	17.2	15.7	14.4
Landsat8	15.4	16	15.3	14.3	16.4	15.9	17.9	16.5	17.6	16.1	15.5	14.4
VIIRS	16.4	17.3	17.3	16.7	16.3	15	18.8	16.8	15.7	16.5	17.4	17.1
SAR	15.4	16.8	16.5	16.1	17.4	15.3	19	16.8	15.6	16.9	16.3	15.1
Dynamic World	16.7	17.6	16.8	16.4	17.6	16.2	18.6	16.6	16.9	18.4	17.9	16.6
Sentinel-2	15.9	16.3	15.4	14.4	16.1	15.7	18.1	16.5	17.6	18	17.6	15.5

Table B.4
Individual Monthly Building MAE for Schema $\mathbf{S}_1$ - Commercial Natural Gas.

Model	1	2	3	4	5	6	7	8	9	10	11	12
Null	101	89.3	80.7	60.1	59.5	64	67.4	68.6	67	63.2	65.2	90.3
NOAA	99.7	88.7	84.1	63.3	44.2	31.3	30.2	30.8	32.9	45.5	71.5	92.9
CMIP	101	90.1	85.4	63.4	43.9	30.8	29.8	30.9	33.7	47.8	72.4	97.8
EPW	101	91.7	84.4	63.7	44.3	31.1	29.4	29.9	32.6	52.7	71.3	94.2
Dynamic World	98.3	88.4	84.6	65.3	50.6	35.7	36.4	40.8	44.3	53.4	72.1	95.4
Landsat8	99.4	88	83.7	61.3	43.5	30.9	29.1	30	31.4	50.9	75.1	96
SAR	102	89	81	60.8	59.8	65.5	67.8	69.9	67.3	63.6	66.2	89.6
VIIRS	100	89.1	82.8	63.3	48.2	61.3	60	66.6	63.1	54.4	67.9	90.9
Sentinel-2	98.5	87.9	85.2	67.6	47	32	29.9	32.1	37.1	51.6	70.2	94.6

Table B.5
Individual Monthly Building MAE for Schema $\mathbf{S}_1$ - Manufacturing Natural Gas.

Model	1	2	3	4	5	6	7	8	9	10	11	12
Null	78	66.4	62.8	54.5	62.7	72.5	73.3	76.2	71.2	66.4	52.3	71.5
NOAA	88.8	75.7	76.4	59.7	40.6	34.5	34.4	35.4	34.6	43.8	58.1	81.2
CMIP	88	74.3	76.7	57.7	38.9	34	34.5	36.4	34.8	43.6	59.7	84.3
EPW	85.7	77.5	77.1	62.5	41.2	35.5	34.4	35.2	34.7	50.8	61	79.5
Dynamic World	80.1	70.4	71.9	59	47.7	40.1	41.5	47.3	54.4	62.7	59.7	79.3
Landsat8	83.7	73.8	74.9	53	41.1	34.6	33.2	34.8	33	51.5	60.7	83
SAR	79.2	67.8	64.3	54.4	61.1	71.9	72	73.4	69	63.7	51.9	73.1
VIIRS	77.5	65.5	65.9	57.2	45.6	64.8	67.1	74	71	58.5	56.7	72.9
Sentinel-2	81.1	75.7	77.8	68	47.7	35	33.1	37.9	43.5	51.8	58.5	83.7

Table B.6
Individual Monthly Building MAE for Schema $\mathbf{S}_1$ - Residential Natural Gas.

Model	1	2	3	4	5	6	7	8	9	10	11	12
Null	112	97.4	85.6	53.8	38.8	44.9	50.1	49.3	47	41	68.3	98.5
NOAA	85.6	75.4	70.2	50.7	34.4	26	23.9	21.4	24.4	37.6	61.2	75.5
CMIP	86.4	76.5	70.4	51.3	34.8	25.9	23.7	21.6	24	38	61.6	75.1
EPW	86.5	76.1	71.7	51.6	35.1	25.9	23.7	21.2	24	41.8	62	76
Dynamic World	89.7	79.8	73.2	55.3	37.5	27	25.7	25.2	29.1	41.1	65.8	76.4
Landsat8	87.5	76.4	71.4	52.8	35.1	26	23.8	21.4	24.3	38.8	60.6	75
SAR	111	97.1	84.5	52.8	38.3	44.5	48.9	49.1	46	40.5	67.2	96.4
VIIRS	106	93.5	81	53.4	36	43.3	43.6	47.6	44.1	39.7	68.9	97.5
Sentinel-2	88.3	76.5	71.4	52.6	36	26.1	23.8	21.8	25.9	39.4	63.6	76.4

Table B.7
Individual Monthly Building MAE for Schema $\mathbf{S}_2$ - Commercial Electricity.

Model	1	2	3	4	5	6	7	8	9	10	11	12
Null	40.5	37	35.4	35.5	40.9	41.6	48	46.4	42.8	39.6	36.9	36.4
NOAA	40.9	36.9	35	35.4	40.5	41.8	47.7	45.6	42.6	40.2	36.7	36.6
CMIP	41.1	37.1	35.1	35.2	40.3	42.3	48.4	46.8	43.3	40.1	36.8	35.9
EPW	41.1	37.7	35.7	35.7	40.9	42.8	48.3	46.6	43.8	41	38	37.2
Landsat8	40.4	36	33.8	33.5	37.4	39.6	45.3	44.3	40.9	38.1	35.9	35.9
VIIRS	40.4	36.7	35.9	35.3	39.8	40	46.6	45.9	41.6	39.4	37.4	39.1
SAR	39.5	36.1	34.6	34.6	39.9	40.1	45.9	45	41.3	38.1	35.4	35.9
Dynamic World	41.5	36.3	34.4	34	39.7	41	46.9	45.7	42.7	39.1	37	40
Sentinel-2	41.3	36.9	35.4	35.2	40.1	42.1	47.2	46.1	43.1	39.9	36.9	37.5

Table B.8
Individual Monthly Building MAE for Schema $\mathbf{S}_2$ - Manufacturing Electricity.

Model	1	2	3	4	5	6	7	8	9	10	11	12
Null	40.5	36.8	43.4	40	43.5	42.8	42.6	43	41.8	42.7	41.5	42.3
NOAA	39.6	35.1	41.2	37.5	40.1	45.7	48.2	48.1	44.2	40.2	37.8	38.8
CMIP	38.6	34.5	40.8	37	40.4	45.5	48.2	47.8	44.8	39.7	38.6	39.3
EPW	40	35	39.8	36.9	39.1	45.7	49.8	50.5	44.4	40.4	37.9	39.4
Landsat8	37.8	33	37.4	33.8	38.3	40.4	45.6	44.7	42.7	37.9	36.8	37.3
VIIRS	42.3	37.1	44	40.6	42.7	43.8	43.5	44	41.8	42.9	42.5	43.2
SAR	39.4	35.9	41.3	38.8	41.6	41	43.3	42	40.8	40.6	39.7	40
Dynamic World	39.3	33.8	38.8	33.9	37.8	39.6	42.3	42.7	40.8	40.1	39	40.7
Sentinel-2	38.3	34	39.6	34.8	38.9	40.3	44.7	46.5	43.4	42.3	38.9	39.3

B2. Individual building results

Tables B.9-B.18

Table B.9
Individual Monthly Building MAE for Schema $\mathbf{S}_2$ - Residential Electricity.

Model	1	2	3	4	5	6	7	8	9	10	11	12
Null	16.7	17.9	17.8	17.6	18.5	15.9	18.7	16.7	16.6	18.8	17.9	16.5
NOAA	15.6	16.6	15.8	15.2	16.4	17	19.2	17.5	17.5	16.9	15.5	14.1
CMIP	15.8	17.2	16.4	16.2	17.6	17.7	19.7	17.9	18.3	17.4	16.5	15
EPW	15.6	16.7	15.3	14.7	16	16.4	19	17.6	17.7	16.7	15.2	13.3
Landsat8	15.3	16	15.3	14.2	16.1	15.3	17.6	16.4	16.7	15.8	15.3	14.7
VIIRS	16.4	17.3	17.3	16.6	16.5	15	18.6	16.6	15.7	16.6	17.5	17.4
SAR	15.1	16.3	16.1	15.6	16.6	15.1	18.8	16.8	15.2	16.3	15.6	14.6
Dynamic World	16.2	17.1	16.1	15.8	16.8	15.9	18.1	16.2	16.5	17.4	17.3	16
Sentinel-2	15.3	16.1	15.3	14.2	15.8	15.6	17.7	16.3	17	17.1	16.4	14.3

Table B.10
Individual Monthly Building MAE for Schema $\mathbf{S}_2$ - Commercial Natural Gas.

Model	1	2	3	4	5	6	7	8	9	10	11	12
Null	101	89.3	80.6	61	60.7	65.6	68.5	70.4	68.1	64.3	66.2	89.2
NOAA	101	90.9	85.3	64.5	44.4	31.4	30.3	31.2	33.4	46.2	72.5	95.3
CMIP	101	90.5	85.2	64.4	43.5	30.5	29.4	30.7	33	44.7	72.5	95
EPW	104	93.4	88	65.5	45	34	30.4	29.9	33.4	50.7	74.7	96.6
Dynamic World	100	91	84.5	65.1	49	36.5	34.6	38.6	42.9	53.9	71.9	95.5
Landsat8	99	88.4	83.4	61.5	43.6	31	29	30.7	31.9	47.3	73.8	94.4
SAR	102	89.4	81.8	61.3	60.2	66.5	56.8	67.6	65.4	63.7	67	89.5
VIIRS	100	88.8	82.1	61.6	47.3	59.3	59.2	64.8	61.2	53.5	66.8	90.6
Sentinel-2	101	90.1	88.1	67.4	47	34.2	31.3	32.6	37	53.1	73.5	95.7

Table B.11
Individual Monthly Building MAE for Schema $\mathbf{S}_2$ - Manufacturing Natural Gas.

Model	1	2	3	4	5	6	7	8	9	10	11	12
Null	78.7	68	63.4	55	61.9	71.8	72.9	75.7	70	65.1	52.2	72.6
NOAA	88.3	76.4	77.3	60.8	40	33.8	34.4	35.2	34.1	43.4	59.2	82.5
CMIP	87.4	75.2	78.4	59.2	38.9	32.6	32.7	34.4	33.6	43.8	61.5	81.9
EPW	88.7	77.6	80.7	59.3	41.7	36.3	34	33.6	34.2	47.4	61.1	78.3
Dynamic World	83.8	72.5	73.5	60.8	46.3	43	42.1	47.1	53.6	65	61.5	83.3
Landsat8	86.2	75.4	75.5	54.7	40.7	34	32.5	36.1	33.2	44.1	61.1	83.1
SAR	78.1	67.5	63.3	54.8	60.8	72.2	62.7	69.3	67.5	65.1	51.8	72.3
VIIRS	76.1	65.1	65.4	57.9	46	64.5	68.5	74.7	72.9	57.6	57.3	74.8
Sentinel-2	82.4	72.2	80.5	64.1	45.5	37.5	35	39.4	43.2	54.1	59.7	80.8

Table B.12
Individual Monthly Building MAE for Schema $\mathbf{S}_2$ - Residential Natural Gas.

Model	1	2	3	4	5	6	7	8	9	10	11	12
Null	112	98	86	54.2	38.8	44.9	49.8	49.4	46.8	41	68.6	98.6
NOAA	86	75.9	70.1	50.6	34.5	25.8	23.7	21.2	24	37.6	61.3	75.2
CMIP	86.6	76.2	71	51.6	35.4	26	24	21.6	24.4	38.1	62.2	77.1
EPW	86.6	76.7	71.9	51.7	35.4	26.3	23.5	21.1	23.9	38.7	61.8	76.2
Dynamic World	88.5	78.2	73.7	54.7	37.2	27.1	25.3	24.1	28.2	40.8	65.2	76.5
Landsat8	86.9	75.3	70.8	51.5	35	26.2	24	21.5	24.2	38.2	60.1	74.6
SAR	110	95.4	83.3	52.6	38.7	45.4	43.3	46.7	44.6	41.3	66.4	92.2
VIIRS	107	94	81.7	53.9	35.6	42.4	43.1	46.7	43.3	39.2	69.5	98.1
Sentinel-2	88.4	77.5	71.1	52.4	36.6	27	24.3	22	26	39.9	63.4	78.4

Table B.13
Individual Monthly Building MAE for Schema $\mathbf{S}_3$ - Commercial Electricity.

Model	1	2	3	4	5	6	7	8	9	10	11	12
Null	39.8	36.3	34.8	35.1	40.4	41.4	47.7	46.2	42.5	39.4	36.1	36.1
NOAA	41.2	37.1	35.3	35.6	40.5	42.3	47.9	45.9	42.7	40.3	36.9	36.2
CMIP	40.9	37.6	35.4	35.1	40.6	41.8	47.9	45.7	43.2	40.2	37	36.5
EPW	40	36.7	34.6	34.8	40.2	41.8	47.9	45.8	43	39.8	36.3	35.9
Landsat8	40	35.7	33.7	33.1	37.2	39.1	45.1	44.1	40.6	38.1	35.4	35.6
VIIRS	40.3	36.7	35.6	35.2	40.3	40.2	47.3	46.1	41.7	39.3	37.1	38.6
SAR	39.4	35.8	34.4	34.8	40.1	39.8	45.8	44.8	41.2	38.2	35.7	35.6
Dynamic World	40.7	36	33.9	32.8	37.8	39.3	45.1	43.8	41	37.4	35.5	37.4
Sentinel-2	40	35.4	34.1	33.7	38.5	40.6	46.3	44.7	41.4	38.1	35.8	36.9

Table B.14
Individual Monthly Building MAE for Schema $\mathbf{S}_3$ - Manufacturing Electricity.

Model	1	2	3	4	5	6	7	8	9	10	11	12
Null	40.8	37.3	43.2	39.9	42.9	42.1	43.1	43.8	41.4	42.4	40.8	42.2
NOAA	39	34.8	40.5	36.2	39.8	45.3	48.1	47.5	43.9	39.6	37.1	38
CMIP	39.9	35.7	40.8	36.7	38.7	44.8	47.6	47.6	43.3	39	38	39.9
EPW	38.6	34.1	39.6	36.5	39.5	44.7	47.4	47.3	42.1	39.5	36.8	38.3
Landsat8	37.5	32.2	37	32.6	36.1	39.6	44.4	44.6	41.3	37.1	36.2	36.9
VIIRS	41.4	37.3	43.9	40.4	41.8	42.9	42.6	42.6	41.6	42.3	42.7	44.8
SAR	39.1	35.6	41.7	38.5	41.7	41.4	42	42	41.2	40.6	39.6	40.7
Dynamic World	37	31.7	36	31.6	35.3	36.1	39.4	40.8	40.3	39	37	38
Sentinel-2	38.9	33.5	38.5	33.3	37.3	41	46.2	45.9	43.3	42.2	39.4	38.9

Table B.15
Individual Monthly Building MAE for Schema $\mathbf{S}_3$ - Residential Electricity.

Model	1	2	3	4	5	6	7	8	9	10	11	12
Null	16.6	17.9	17.7	17.5	18.5	15.9	18.9	16.8	16.6	18.7	17.7	16.6
NOAA	15.8	16.8	15.9	15.2	16.6	16.9	19.4	17.7	17.6	16.8	15.5	13.9
CMIP	15.5	16.7	15.7	15.2	16.1	16.9	18.9	17.5	17.3	16.7	15.6	14.3
EPW	15.8	17.1	16.1	15.7	16.8	17.2	19.2	17.8	17.8	17.5	16	14.5
Landsat8	14.9	15.6	14.8	14	15.5	15.1	17.6	16.1	16.5	15.4	14.6	13.9
VIIRS	16.4	17.5	17.3	16.6	16.6	15.1	18.7	16.8	15.7	16.7	17.1	17
SAR	15.4	16.7	16.3	15.9	17.3	15.3	18.7	16.6	15.7	16.8	16.1	14.9
Dynamic World	15.7	16.5	15.6	15.1	15.7	16	18	16.3	16.5	16.4	16.3	15
Sentinel-2	15.6	16.3	15.5	14.2	15.8	15.7	18	16.8	17.5	17.5	16.8	14.2

Table B.16
Individual Monthly Building MAE for Schema $\mathbf{S}_3$ - Commercial Natural Gas.

Model	1	2	3	4	5	6	7	8	9	10	11	12
Null	101	88.8	80.3	60.7	60.7	65.7	68.8	70.5	68.3	64.5	65.2	89.4
NOAA	99.9	89.6	84.1	62.8	43.3	30.3	28.8	29.2	31.8	44.3	71.4	93.7
CMIP	99.7	89.8	82.7	61.6	43.3	30.1	28.3	28.8	32.3	45.7	70.8	93.9
EPW	102	92.9	87.8	65.7	44.9	31.4	28.5	28.7	31.7	48.2	73.3	94.2
Dynamic World	98.1	88.8	82.8	62.8	47.1	35.2	34.5	37.9	42.3	52.1	70.2	92.5
Landsat8	101	91.6	85.6	62.9	45.6	32.7	30.3	31.5	33.2	49.5	75.2	97.3
SAR	100	88.6	80.2	59.9	59	65.9	55.9	66.8	64	63	66	89.8
VIIRS	101	89.4	82.4	62.2	46.1	58	57.6	63.4	59.6	52.4	66.6	91.6
Sentinel-2	101	88.3	84.9	64.3	44.2	31.5	28.3	30	34.8	48.6	71.4	94.8

Table B.17
Individual Monthly Building MAE for Schema $\mathbf{S}_3$ - Manufacturing Natural Gas.

Model	1	2	3	4	5	6	7	8	9	10	11	12
Null	79.2	68.4	64.1	54.6	62	71.1	72.3	74.2	69	65.1	52.5	73.7
NOAA	87	74.5	74.7	57.4	39.4	34.2	33.5	34.3	33.5	42.1	58.6	80.1
CMIP	87.1	76.3	77.3	57.5	39.3	33.7	31.9	33.1	33.5	43.3	58.7	81.4
EPW	84.6	75.5	76	60.3	41.7	35	33	32.9	32.3	45.5	60.4	77.3
Dynamic World	80	68.6	70.2	57	47.4	41.1	40.8	46.8	53.3	63.1	57.3	78.6
Landsat8	85.9	75.5	73	54.6	43.7	36.7	34.7	37.7	34.6	47.1	60.4	83.4
SAR	79.9	68.1	64.6	54.9	58.7	70.7	61	67.4	65.7	62.9	52.7	73.9
VIIRS	78.5	66.4	67.8	59.3	47	64.6	69.2	75.3	73.3	59.7	57.4	74.9
Sentinel-2	81.6	72.9	77.7	63.8	39.8	33.6	31.3	34.3	40.2	51.7	57.7	81.9

Table B.18
Individual Monthly Building MAE for Schema $\mathbf{S}_3$ - Residential Natural Gas.

Model	1	2	3	4	5	6	7	8	9	10	11	12
Null	112	97.9	86	53.8	39.1	45.4	50.4	49.9	47.3	41.3	68.6	98.7
NOAA	84.7	74.4	69.6	50.6	34.4	25.8	23.6	21.4	24	37.2	60.9	74.6
CMIP	85.2	74.6	69.9	51.3	34.8	25.7	23.4	21	24	37.9	61.6	75.9
EPW	86.1	76.2	71.2	51.8	35	25.7	23.5	20.9	23.8	39.3	61.2	76.6
Dynamic World	88.8	78.2	73	54.4	36	26.2	24.6	23.5	27.3	40.4	64.5	76.2
Landsat8	88.1	76.5	71.4	52.4	35.4	26.2	24.2	21.9	24.7	38.4	60.7	75.3
SAR	109	95.4	82.9	52.3	38.3	45.4	42.9	46.1	44.2	41.2	65.9	91.8
VIIRS	107	94.2	81.5	53.8	36.3	42.9	43.2	46.9	43.5	39.6	69.4	98.1
Sentinel-2	86.4	76.5	70.6	51.9	35.5	26.4	23.8	21.1	25	39.3	62.3	77.2

Table B.19
Individual Building Results for Schema $\mathbf{S}_1$.

Energy Class	Model	CV(RMSE)	NMBE	MAE	CV(STD)	RMSE
Electricity	VIIRS	94.01	−0.8161	25.79	65.26	50.17
Electricity	SAR	94.22	1.381	25.56	65.26	50.28
Electricity	Sentinel-2	94.27	−0.1591	25.58	65.26	50.3
Electricity	Landsat8	94.41	0.361	25.25	65.26	50.38
Electricity	Dynamic World	95.3	−0.1949	26.06	65.26	50.85
Electricity	NOAA	95.81	−0.3424	25.72	65.26	51.13
Electricity	CMIP	96.74	−2.388	26.47	65.26	51.63
Electricity	EPW	96.88	−1.624	26.24	65.26	51.7
Electricity	Null	97.56	0.4302	26.54	65.26	52.06
Natural Gas	NOAA	115	2.838	50.04	71.38	87.05
Natural Gas	CMIP	115.2	1.427	50.46	71.38	87.26
Natural Gas	EPW	115.5	0.1371	50.92	71.38	87.46
Natural Gas	Landsat8	115.9	3.42	50.49	71.38	87.73
Natural Gas	Sentinel-2	116.4	2.218	51.54	71.38	88.11
Natural Gas	Dynamic World	119.8	2.438	53.78	71.38	90.71
Natural Gas	VIIRS	128.1	1.143	62.83	71.38	97
Natural Gas	SAR	129.9	0.5474	65.22	71.38	98.37
Natural Gas	Null	130.6	1.145	65.56	71.38	98.92

B3. Aggregated results

Tables B.20, B.22, B.23, B.25, B.26, B.27.

Table B.20
Individual Building Results for Schema $\mathbf{S}_2$.

Energy Class	Model	CV(RMSE)	NMBE	MAE	CV(STD)	RMSE
Electricity	Landsat8	93.1	1.477	24.76	65.26	49.68
Electricity	VIIRS	93.6	−1.088	25.97	65.26	49.95
Electricity	SAR	93.85	1.967	25.18	65.26	50.08
Electricity	Dynamic World	95.44	−0.693	25.78	65.26	50.93
Electricity	NOAA	95.76	−0.4093	25.97	65.26	51.1
Electricity	Sentinel-2	95.78	1.646	25.6	65.26	51.11
Electricity	Null	96.72	0.2819	26.56	65.26	51.62
Electricity	EPW	96.76	−1.207	26.08	65.26	51.64
Electricity	CMIP	97.31	−0.4502	26.47	65.26	51.93
Natural Gas	Landsat8	115.1	3.197	50.1	71.38	87.16
Natural Gas	NOAA	115.4	2.393	50.29	71.38	87.4
Natural Gas	EPW	115.9	−0.9957	51.26	71.38	87.74
Natural Gas	CMIP	116.1	0.9616	50.5	71.38	87.88
Natural Gas	Sentinel-2	117.4	1.153	52.21	71.38	88.87
Natural Gas	Dynamic World	119.7	1.096	53.45	71.38	90.6
Natural Gas	VIIRS	128	3.495	62.45	71.38	96.9
Natural Gas	SAR	128.9	1.157	63.99	71.38	97.6
Natural Gas	Null	131.6	0.6646	65.89	71.38	99.63

Table B.21
Individual Building Results for Schema $\mathbf{S}_3$.

Energy Class	Model	CV(RMSE)	NMBE	MAE	CV(STD)	RMSE
Electricity	Landsat8	92.58	2.102	24.42	65.26	49.4
Electricity	SAR	93.41	1.423	25.34	65.26	49.85
Electricity	Dynamic World	93.9	2.243	24.87	65.26	50.11
Electricity	Sentinel-2	94.01	−0.2982	25.27	65.26	50.17
Electricity	VIIRS	94.46	0.2878	25.99	65.26	50.41
Electricity	NOAA	95.94	−0.5896	26.04	65.26	51.2
Electricity	CMIP	96.17	−0.0328	25.94	65.26	51.32
Electricity	EPW	96.51	−0.4866	26.05	65.26	51.5
Electricity	Null	97.03	1.104	26.4	65.26	51.78
Natural Gas	NOAA	114.3	2.472	49.56	71.38	86.59
Natural Gas	CMIP	114.5	1.811	49.7	71.38	86.69
Natural Gas	EPW	115.5	0.09753	50.64	71.38	87.47
Natural Gas	Sentinel-2	115.8	2.914	50.75	71.38	87.68
Natural Gas	Landsat8	115.9	1.43	51.06	71.38	87.73
Natural Gas	Dynamic World	117.9	3.662	52.51	71.38	89.26
Natural Gas	VIIRS	128.3	4.012	62.45	71.38	97.12
Natural Gas	SAR	128.4	1.683	63.45	71.38	97.22
Natural Gas	Null	131.1	0.07637	65.98	71.38	99.26

Table B.22
Aggregated Building Results for Schema $\mathbf{S}_1$.

Energy Class	Model	CV(RMSE)	NMBE	MAE	CV(STD)	RMSE
Electricity	Landsat8	27.01	−9.299	72.95	350.6	86.61
Electricity	NOAA	27.21	−10.31	73.27	350.6	81.25
Electricity	Sentinel-2	28.58	−7.669	74.96	350.6	85.67
Electricity	EPW	28.63	−11.3	77.21	350.6	89.44
Electricity	SAR	29.06	−5.232	76.87	350.6	93.86
Electricity	CMIP	29.39	−14.17	71.43	350.6	88.65
Electricity	Dynamic World	30.56	−8.163	85.37	350.6	95.62
Electricity	VIIRS	31.3	−8.132	84.8	350.6	97.36
Electricity	Null	31.41	−8.751	78.07	350.6	93.07
Natural Gas	EPW	41.5	−5.591	153.3	141	203.4
Natural Gas	CMIP	42.63	−4.474	148.4	141	191
Natural Gas	NOAA	44.82	−3.33	133.5	141	179.4
Natural Gas	Landsat8	46.51	−2.409	150.4	141	188.8
Natural Gas	Sentinel-2	48.24	−2.017	159.6	141	211.3
Natural Gas	Dynamic World	48.95	−1.401	185	141	220.9
Natural Gas	VIIRS	71.75	−1.378	262.2	141	307.7
Natural Gas	Null	76.94	−4.749	274.6	141	323.7
Natural Gas	SAR	79.19	−5.245	274.3	141	323.6

Table B.23
Aggregated Building Results for Schema $\mathbf{S}_2$.

Energy Class	Model	CV(RMSE)	NMBE	MAE	CV(STD)	RMSE
Electricity	Landsat8	25.98	−5.899	72.71	350.6	83.3
Electricity	EPW	28.37	−8.728	71.93	350.6	80.63
Electricity	NOAA	28.56	−10.17	76.15	350.6	87.3
Electricity	CMIP	28.57	−12.9	73.78	350.6	85.17
Electricity	Dynamic World	28.71	−8.081	80.2	350.6	93.86
Electricity	SAR	28.84	−4.483	74.28	350.6	88.93
Electricity	Sentinel-2	29.03	−5.309	80.1	350.6	90.11
Electricity	VIIRS	31.22	−10.73	79.99	350.6	95.42
Electricity	Null	31.51	−9.297	80.04	350.6	93.67
Natural Gas	CMIP	42.28	−4.95	145.5	141	194
Natural Gas	Landsat8	43.42	−0.1227	145.2	141	190.6
Natural Gas	EPW	44.21	−7.446	156.7	141	196.9
Natural Gas	NOAA	45.13	−4.095	137.5	141	179
Natural Gas	Sentinel-2	49.13	−5.049	170.8	141	209.9
Natural Gas	Dynamic World	50.16	−3.409	172.4	141	214.9
Natural Gas	VIIRS	71.41	−2.03	257.6	141	307.2
Natural Gas	SAR	74.12	−4.754	265.9	141	331.5
Natural Gas	Null	78.92	−6.163	275.6	141	333.7

Table B.24
Aggregated Building Results for Schema $\mathbf{S}_3$.

Energy Class	Model	CV(RMSE)	NMBE	MAE	CV(STD)	RMSE
Electricity	Landsat8	25.7	−6.813	69.19	350.6	79.49
Electricity	Dynamic World	26.65	−4.752	70.12	350.6	85.51
Electricity	Sentinel-2	26.95	−8.267	77.69	350.6	84.4
Electricity	NOAA	27.68	−11.47	72.87	350.6	81.94
Electricity	EPW	28.26	−10.49	72.63	350.6	84.19
Electricity	CMIP	28.42	−9.798	76.31	350.6	85.54
Electricity	SAR	29.13	−6.787	76.86	350.6	92.88
Electricity	VIIRS	31.62	−8.535	79.7	350.6	95.15
Electricity	Null	31.88	−8.094	78.78	350.6	95.74
Natural Gas	NOAA	42.52	−1.922	135.1	141	179.6
Natural Gas	CMIP	43.1	−3.032	132.7	141	167.4
Natural Gas	EPW	44.3	−5.405	146.6	141	189.9
Natural Gas	Landsat8	45.65	−3.373	156.5	141	198.4
Natural Gas	Dynamic World	46.1	−0.3658	170.4	141	215.3
Natural Gas	Sentinel-2	46.23	−2.027	150.1	141	192.8
Natural Gas	VIIRS	70.54	−1.666	249.3	141	307.1
Natural Gas	SAR	74.13	−2.701	264.5	141	312.5
Natural Gas	Null	77.5	−5.936	274	141	329.3

Table B.25
Individual Building Results by Zone for Schema $\mathbf{S}_1$.

Energy Class	Zone	Model	CV(RMSE)	NMBE	CV(STD)	RMSE	MAE
Electricity	Commercial	SAR	79.12	9.463	78.14	65.32	39.36
Electricity	Commercial	VIIRS	79.19	6.623	78.14	65.38	39.46
Electricity	Commercial	Sentinel-2	79.25	9.735	78.14	65.43	39.5
Electricity	Commercial	Landsat8	79.78	8.726	78.14	65.86	39.54
Electricity	Commercial	Dynamic World	80.02	10.12	78.14	66.07	39.58
Electricity	Commercial	CMIP	80.77	9.118	78.14	66.68	40.35
Electricity	Commercial	NOAA	81.08	9.611	78.14	66.94	39.86
Electricity	Commercial	Null	81.22	11.44	78.14	67.06	40.15
Electricity	Commercial	EPW	81.98	9.139	78.14	67.68	40.69
Electricity	Manufacturing	Landsat8	122.6	−34.79	77.07	50.58	39.12
Electricity	Manufacturing	NOAA	124.1	−38.87	77.07	51.2	40.66
Electricity	Manufacturing	CMIP	124.2	−44.43	77.07	51.22	40.64
Electricity	Manufacturing	Sentinel-2	125.2	−38.02	77.07	51.65	40.31
Electricity	Manufacturing	Dynamic World	125.9	−40.14	77.07	51.95	40.8
Electricity	Manufacturing	EPW	126.8	−42.41	77.07	52.3	41.46
Electricity	Manufacturing	Null	127.9	−38.26	77.07	52.76	41.5
Electricity	Manufacturing	VIIRS	130.6	−39.57	77.07	53.88	42.14
Electricity	Manufacturing	SAR	130.8	−36.38	77.07	53.97	41.05
Electricity	Residential	VIIRS	102.1	−6.586	61.95	38.64	16.75
Electricity	Residential	SAR	102.8	−5.269	61.95	38.92	16.51
Electricity	Residential	Landsat8	103	−6.867	61.95	38.98	16.06
Electricity	Residential	Sentinel-2	103.4	−9.035	61.95	39.12	16.53
Electricity	Residential	NOAA	104.3	−9.233	61.95	39.48	16.53
Electricity	Residential	Dynamic World	104.8	−9.405	61.95	39.65	17.24
Electricity	Residential	EPW	105.4	−11.31	61.95	39.87	16.86
Electricity	Residential	CMIP	107.7	−12.88	61.95	40.77	17.48
Electricity	Residential	Null	108.8	−9.749	61.95	41.17	17.65
Natural Gas	Commercial	CMIP	151.3	−21.37	58.14	95.31	57.86
Natural Gas	Commercial	Landsat8	151.5	−17.54	58.14	95.41	57.32
Natural Gas	Commercial	NOAA	151.5	−18.37	58.14	95.42	57.01
Natural Gas	Commercial	EPW	152	−21.51	58.14	95.73	57.99
Natural Gas	Commercial	Sentinel-2	153.8	−19.73	58.14	96.91	58.73
Natural Gas	Commercial	Dynamic World	157.2	−20.73	58.14	99.04	61.44
Natural Gas	Commercial	VIIRS	166.1	−20.92	58.14	104.6	68.94
Natural Gas	Commercial	Null	168.9	−20.86	58.14	106.4	71.66
Natural Gas	Commercial	SAR	170.1	−22.15	58.14	107.1	72.2
Natural Gas	Manufacturing	CMIP	174.9	−20.18	52.65	97.77	54.68
Natural Gas	Manufacturing	NOAA	175.4	−21.23	52.65	98.04	54.84
Natural Gas	Manufacturing	Landsat8	176	−16.72	52.65	98.39	54.39
Natural Gas	Manufacturing	EPW	176.9	−24.29	52.65	98.91	56.18
Natural Gas	Manufacturing	Sentinel-2	178.7	−24.31	52.65	99.88	57.73
Natural Gas	Manufacturing	Dynamic World	181	−23.5	52.65	101.2	59.38
Natural Gas	Manufacturing	VIIRS	187.5	−21.12	52.65	104.8	63.78
Natural Gas	Manufacturing	SAR	189	−17.47	52.65	105.6	65.77
Natural Gas	Manufacturing	Null	189	−20.79	52.65	105.7	66.33
Natural Gas	Residential	NOAA	97.88	11.94	80.15	81.69	46.23
Natural Gas	Residential	EPW	98.39	9.419	80.15	82.12	47.03
Natural Gas	Residential	CMIP	98.4	11.01	80.15	82.12	46.49
Natural Gas	Residential	Sentinel-2	98.78	11.71	80.15	82.44	47.53
Natural Gas	Residential	Landsat8	99.22	12.24	80.15	82.8	46.82
Natural Gas	Residential	Dynamic World	102.4	12.36	80.15	85.44	49.58
Natural Gas	Residential	VIIRS	110.7	10.48	80.15	92.37	59.73
Natural Gas	Residential	SAR	111.6	9.917	80.15	93.15	61.71
Natural Gas	Residential	Null	113.2	10.44	80.15	94.46	62.47

Table B.26
Individual Building Results by Zone for Schema $\mathbf{S}_2$.

Energy Class	Zone	Model	CV(RMSE)	NMBE	CV(STD)	RMSE	MAE
Electricity	Commercial	Landsat8	78.28	10.03	78.14	64.63	38.65
Electricity	Commercial	SAR	78.93	9.259	78.14	65.17	39.09
Electricity	Commercial	VIIRS	79.66	6.834	78.14	65.76	39.97
Electricity	Commercial	Dynamic World	81.05	7.678	78.14	66.91	39.99
Electricity	Commercial	Null	81.3	11.49	78.14	67.12	40.38
Electricity	Commercial	EPW	81.62	8.005	78.14	67.39	41.05
Electricity	Commercial	NOAA	81.67	10.06	78.14	67.42	40.32
Electricity	Commercial	Sentinel-2	82.25	10.56	78.14	67.9	40.39
Electricity	Commercial	CMIP	82.55	11.7	78.14	68.15	40.55
Electricity	Manufacturing	Dynamic World	122.2	−34.2	77.07	50.4	38.99
Electricity	Manufacturing	Landsat8	122.9	−28.71	77.07	50.71	38.83
Electricity	Manufacturing	NOAA	126	−40.67	77.07	51.98	41.42
Electricity	Manufacturing	Sentinel-2	126.2	−34.31	77.07	52.05	40.12
Electricity	Manufacturing	CMIP	126.3	−44.73	77.07	52.08	41.32
Electricity	Manufacturing	SAR	127.1	−34.41	77.07	52.41	40.4
Electricity	Manufacturing	EPW	128.1	−40.7	77.07	52.84	41.55
Electricity	Manufacturing	Null	128.2	−40.68	77.07	52.89	41.75
Electricity	Manufacturing	VIIRS	130.6	−41.84	77.07	53.85	42.35
Electricity	Residential	VIIRS	99.88	−7.279	61.95	37.8	16.75
Electricity	Residential	Sentinel-2	101.5	−6.193	61.95	38.41	16.07
Electricity	Residential	Landsat8	102.2	−6.422	61.95	38.66	15.79
Electricity	Residential	SAR	102.6	−3.831	61.95	38.81	16.09
Electricity	Residential	NOAA	102.7	−9.788	61.95	38.87	16.62
Electricity	Residential	Dynamic World	103.5	−8.073	61.95	39.17	16.69
Electricity	Residential	CMIP	105.5	−11.54	61.95	39.93	17.31
Electricity	Residential	EPW	105.6	−9.098	61.95	39.96	16.38
Electricity	Residential	Null	106.1	−9.942	61.95	40.16	17.52
Natural Gas	Commercial	Landsat8	150.4	−18.21	58.14	94.74	56.88
Natural Gas	Commercial	CMIP	150.9	−21.34	58.14	95.06	57.33
Natural Gas	Commercial	NOAA	152.8	−19.86	58.14	96.26	57.88
Natural Gas	Commercial	EPW	153.4	−25.76	58.14	96.62	59.51
Natural Gas	Commercial	Sentinel-2	156	−23.46	58.14	98.24	60.14
Natural Gas	Commercial	Dynamic World	158.5	−21.78	58.14	99.82	61.25
Natural Gas	Commercial	VIIRS	164.2	−17.07	58.14	103.4	67.88
Natural Gas	Commercial	SAR	169.3	−20.61	58.14	106.6	71.11
Natural Gas	Commercial	Null	170.8	−22.7	58.14	107.6	72.43
Natural Gas	Manufacturing	NOAA	177	−19.48	52.65	98.94	55.05
Natural Gas	Manufacturing	CMIP	177	−21.22	52.65	98.95	54.61
Natural Gas	Manufacturing	EPW	177.3	−22.67	52.65	99.11	55.95
Natural Gas	Manufacturing	Landsat8	177.4	−15.75	52.65	99.18	54.14
Natural Gas	Manufacturing	Sentinel-2	180.4	−23.09	52.65	100.9	57.84
Natural Gas	Manufacturing	Dynamic World	183.3	−26.45	52.65	102.5	60.91
Natural Gas	Manufacturing	VIIRS	187.2	−22.3	52.65	104.6	64.05
Natural Gas	Manufacturing	SAR	188.4	−15.64	52.65	105.3	64.64
Natural Gas	Manufacturing	Null	190.7	−18.48	52.65	106.6	66.21
Natural Gas	Residential	NOAA	97.91	11.78	80.15	81.72	46.18
Natural Gas	Residential	EPW	98.32	9.323	80.15	82.06	46.82
Natural Gas	Residential	Landsat8	98.46	12.13	80.15	82.17	46.45
Natural Gas	Residential	Sentinel-2	99.27	11.54	80.15	82.85	47.87
Natural Gas	Residential	CMIP	99.69	10.38	80.15	83.2	46.81
Natural Gas	Residential	Dynamic World	101.5	10.99	80.15	84.7	49.05
Natural Gas	Residential	SAR	110.5	10.12	80.15	92.18	60.41
Natural Gas	Residential	VIIRS	111.3	12.44	80.15	92.89	59.64
Natural Gas	Residential	Null	113.7	10.34	80.15	94.9	62.62

Table B.27
Individual Building Results by Zone for Schema $\mathbf{S}_3$.

Energy Class	Zone	Model	CV(RMSE)	NMBE	CV(STD)	RMSE	MAE
Electricity	Commercial	Landsat8	77.77	9.675	78.14	64.21	38.38
Electricity	Commercial	Dynamic World	78.48	9.921	78.14	64.79	38.55
Electricity	Commercial	Sentinel-2	78.84	8.75	78.14	65.09	39.02
Electricity	Commercial	SAR	79.19	9.537	78.14	65.38	39.06
Electricity	Commercial	VIIRS	80.39	8.637	78.14	66.37	40.03
Electricity	Commercial	EPW	80.78	10.61	78.14	66.69	40.09
Electricity	Commercial	Null	80.97	11.79	78.14	66.84	39.96
Electricity	Commercial	CMIP	81.1	10.2	78.14	66.96	40.46
Electricity	Commercial	NOAA	81.39	9.737	78.14	67.19	40.49
Electricity	Manufacturing	Dynamic World	116.6	−28.07	77.07	48.1	36.83
Electricity	Manufacturing	Landsat8	119.4	−27.73	77.07	49.27	37.93
Electricity	Manufacturing	SAR	124.7	−35.63	77.07	51.42	40.34
Electricity	Manufacturing	EPW	125	−38.26	77.07	51.54	40.39
Electricity	Manufacturing	NOAA	125.4	−39.51	77.07	51.74	40.88
Electricity	Manufacturing	CMIP	125.9	−40.25	77.07	51.93	40.97
Electricity	Manufacturing	Sentinel-2	126	−36.41	77.07	51.98	39.94
Electricity	Manufacturing	VIIRS	127.2	−43.02	77.07	52.46	41.95
Electricity	Manufacturing	Null	129.8	−35.07	77.07	53.56	41.62
Electricity	Residential	SAR	101	−5.33	61.95	38.22	16.38
Electricity	Residential	VIIRS	101.4	−6.206	61.95	38.35	16.78
Electricity	Residential	Landsat8	102.1	−4.617	61.95	38.62	15.44
Electricity	Residential	Sentinel-2	103.4	−8.284	61.95	39.11	16.31
Electricity	Residential	NOAA	103.9	−9.905	61.95	39.33	16.69
Electricity	Residential	Dynamic World	104.8	−4.563	61.95	39.67	16.18
Electricity	Residential	CMIP	105.2	−9.12	61.95	39.79	16.52
Electricity	Residential	EPW	106.9	−10.85	61.95	40.46	16.96
Electricity	Residential	Null	107.6	−8.893	61.95	40.7	17.5
Natural Gas	Commercial	CMIP	149.4	−19.98	58.14	94.1	56.27
Natural Gas	Commercial	NOAA	150.9	−17.91	58.14	95.04	56.43
Natural Gas	Commercial	Landsat8	152.6	−22.25	58.14	96.14	58.68
Natural Gas	Commercial	Sentinel-2	152.7	−18.65	58.14	96.22	57.6
Natural Gas	Commercial	EPW	153.3	−21.11	58.14	96.56	58.2
Natural Gas	Commercial	Dynamic World	155.4	−17.33	58.14	97.87	59.72
Natural Gas	Commercial	VIIRS	164.2	−14.46	58.14	103.4	67.34
Natural Gas	Commercial	SAR	168	−19.26	58.14	105.8	70.08
Natural Gas	Commercial	Null	169.3	−23.53	58.14	106.6	72.33
Natural Gas	Manufacturing	NOAA	176.3	−17.31	52.65	98.56	53.65
Natural Gas	Manufacturing	CMIP	177.4	−18.34	52.65	99.19	54.04
Natural Gas	Manufacturing	EPW	177.5	−22.8	52.65	99.21	54.41
Natural Gas	Manufacturing	Landsat8	177.9	−17.15	52.65	99.47	55.02
Natural Gas	Manufacturing	Dynamic World	178.5	−24.1	52.65	99.78	58.5
Natural Gas	Manufacturing	Sentinel-2	178.6	−19.03	52.65	99.86	55.53
Natural Gas	Manufacturing	VIIRS	187.3	−24.5	52.65	104.7	65.18
Natural Gas	Manufacturing	SAR	188.3	−13.44	52.65	105.3	64.2
Natural Gas	Manufacturing	Null	191.8	−16.89	52.65	107.2	66.15
Natural Gas	Residential	NOAA	97.17	11.06	80.15	81.09	45.85
Natural Gas	Residential	EPW	97.81	9.144	80.15	81.63	46.62
Natural Gas	Residential	CMIP	97.95	10.94	80.15	81.75	46.13
Natural Gas	Residential	Sentinel-2	98.4	12.05	80.15	82.13	47.01
Natural Gas	Residential	Landsat8	98.59	11.2	80.15	82.28	47
Natural Gas	Residential	Dynamic World	100.4	12.86	80.15	83.82	48.5
Natural Gas	Residential	SAR	110.3	10.26	80.15	92.04	60.11
Natural Gas	Residential	VIIRS	111.7	12.3	80.15	93.24	59.82
Natural Gas	Residential	Null	113.6	9.737	80.15	94.77	62.82

B4. Individual building results by zone

Figures B.1 and B.2

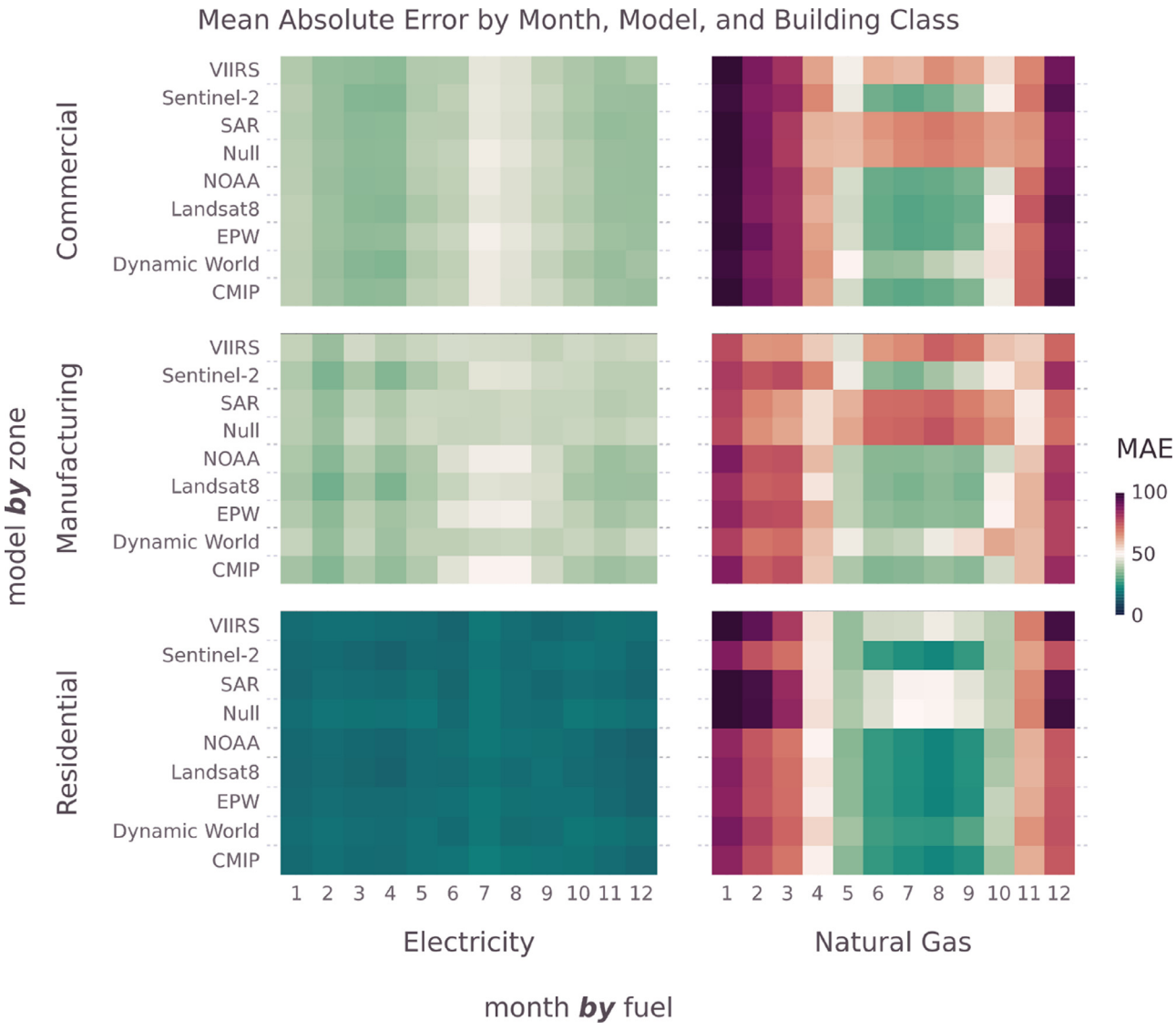

Fig. B.1. MAE bins showing mean absolute error by month, model, and building class. From schema $\mathbf{S}_1$.

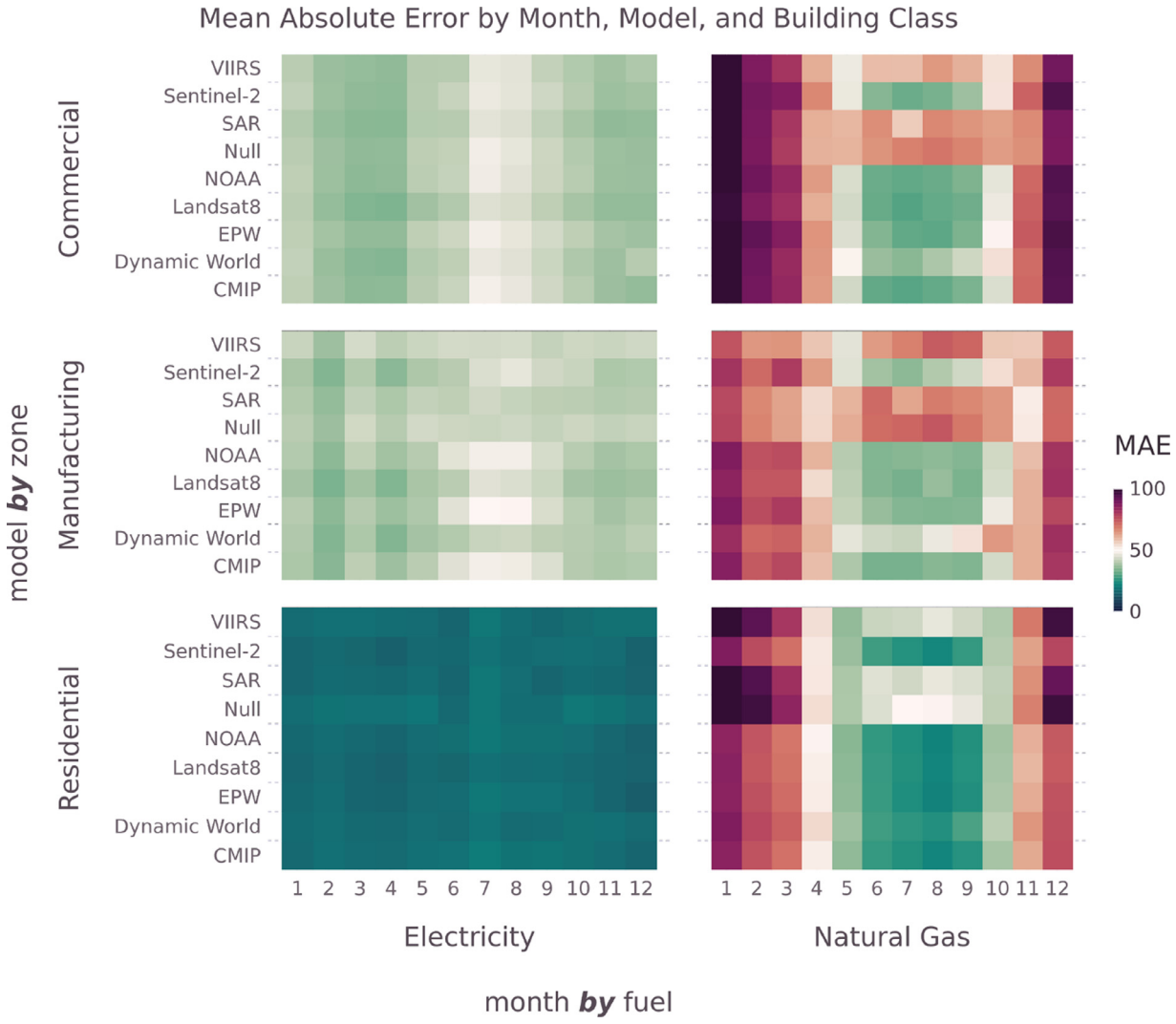

Fig. B.2. MAE bins showing mean absolute error by month, model, and building class. From schema $\mathbf{S}_2$.

B5. Monthly errors - Mean absolute value

Figures B.3

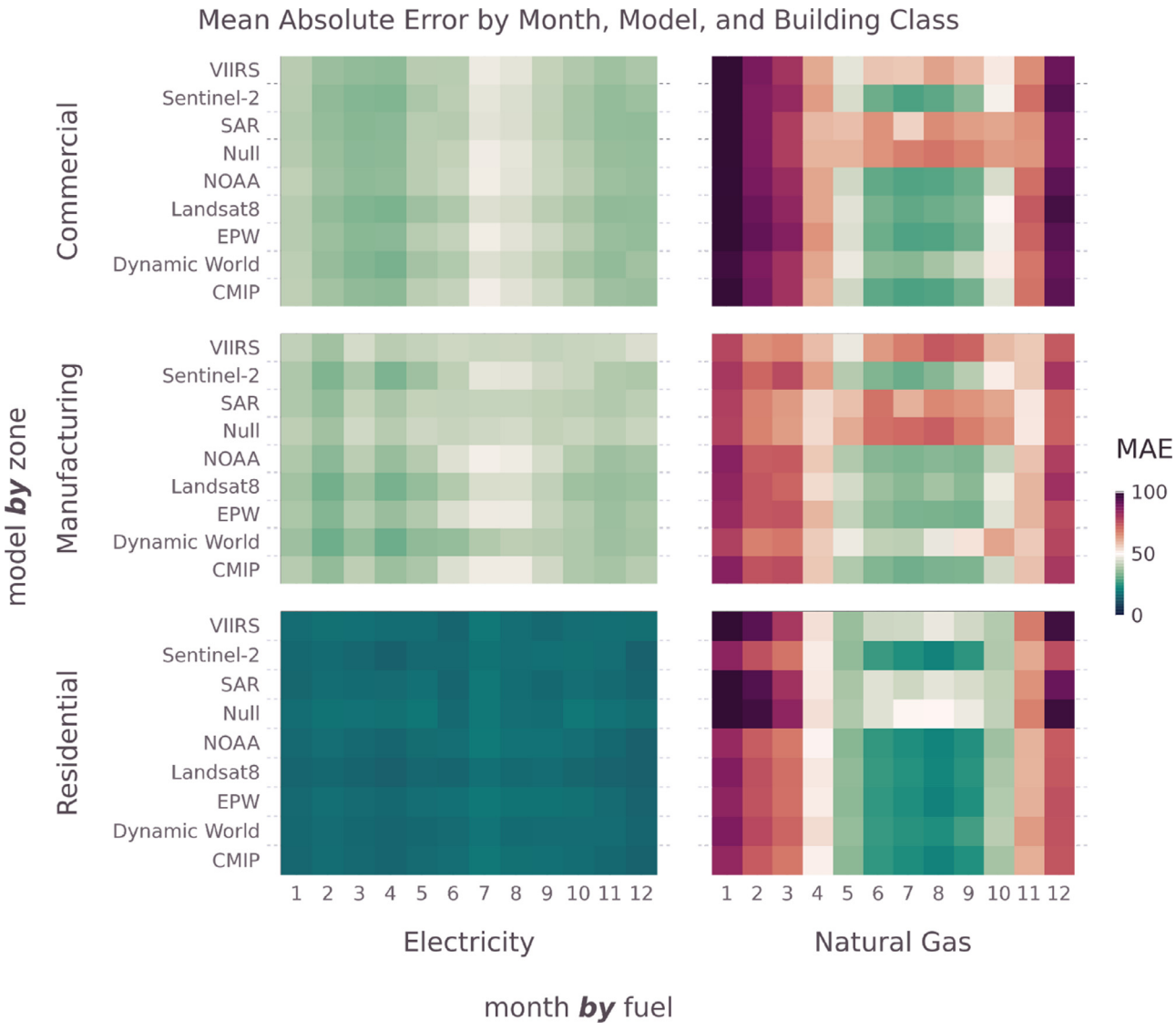

Fig. B.3. MAE bins showing mean absolute error by month, model, and building class. From schema $\mathbf{S}_3$.

References

[1] Reinhart CF, Cerezo Davila C. Urban building energy modeling – a review of a nascent field. Build Environ 2016;97:196–202. doi:10.1016/j.buildenv.2015.12.001. https://www.sciencedirect.com/science/article/pii/S0360132315003248

[2] Cerezo C, Sokol J, AlKhaled S, Reinhart C, Al-Mumin A, Hajiah A. Comparison of four building archetype characterization methods in urban building energy modeling (UBEM): aresidential case study in kuwait city. Energy Build 2017;154:321–34. doi:10.1016/j.enbuild.2017.08.029. https://www.sciencedirect.com/science/article/pii/S0378778817314743

[3] Nagpal S, Mueller C, Aijazi A, Reinhart CF. A methodology for auto-calibrating urban building energy models using surrogate modeling techniques. J Build Perform Simul 2019;12(1):1–16. Publisher: Taylor & Francis _eprint: doi: 10.1080/19401493.2018.1457722.

[4] Craig MT, Wohland J, Stoop LP, Kies A, Pickering B, Bloomfield HC, Browell J, De Felice M, Dent CJ, Deroubaix A, Frischmuth F, Gonzalez PLM, Grochowicz A, Gruber K, Härtel P, Kittel M, Kotzur L, Labuhn I, Lundquist JK, Pflugradt N, van der Wiel K, Zeyringer M, Brayshaw DJ. Overcoming the disconnect between energy system and climate modeling. Joule 2022;6(7):1405–17. doi:10.1016/j.joule.2022.05.010. https://www.sciencedirect.com/science/article/pii/S2542435122002379

[5] Javanroodi K, Nik VM. Impacts of microclimate conditions on the energy performance of buildings in urban areas. Buildings 2019;9(8):189. doi:10.3390/buildings9080189. Number: 8 Publisher: Multidisciplinary Digital Publishing Institute

[6] Huang K, Li X, Liu X, Seto KC. Projecting global urban land expansion and heat island intensification through 2050. Environ Res Lett 2019;14(11):114037. doi:10.1088/1748-9326/ab4b71. Publisher: IOP Publishing

[7] Luo X, Hong T, Tang Y-H. Modeling thermal interactions between buildings in an urban context. Energies 2020;13(9):2382. doi:10.3390/en13092382. Number: 9 Publisher: Multidisciplinary Digital Publishing Institute

[8] Zhang M, Gao Z. Effect of urban form on microclimate and energy loads: case study of generic residential district prototypes in Nanjing, China. Sustain Cities Soc 2021;70:102930. doi:10.1016/j.scs.2021.102930. https://www.sciencedirect.com/science/article/pii/S221067072100216X

[9] Hadavi M, Pasdarshahri H. Investigating effects of urban configuration and density on urban climate and building systems energy consumption. J Build Eng 2021;44:102710. doi:10.1016/j.jobe.2021.102710. https://www.sciencedirect.com/science/article/pii/S2352710221005684

[10] Fung WY, Lam KS, Hung WT, Pang SW, Lee YL. Impact of urban temperature on energy consumption of Hong Kong. Energy 2006;31(14):2623–37. doi:10.1016/j.energy.2005.12.009. https://www.sciencedirect.com/science/article/pii/S0360544206000119

[11] Toparlar Y, Blocken B, Maiheu B, van Heijst GJF. Impact of urban microclimate on summertime building cooling demand: a parametric analysis for Antwerp, Belgium. Appl Energy 2018;228:852–72. doi:10.1016/j.apenergy.2018.06.110. https://www.sciencedirect.com/science/article/pii/S0306261918309814

[12] Khoshdel Nikkho S, Heidarinejad M, Liu J, Srebric J. Quantifying the impact of urban wind sheltering on the building energy consumption. Appl Therm Eng 2017;116:850–65. doi:10.1016/j.applthermaleng.2017.01.044. https://www.sciencedirect.com/science/article/pii/S1359431117302843

[13] Oke TR. Street design and urban canopy layer climate. Energy Build 1988;11(1):103–13. doi:10.1016/0378-7788(88)90026-6. https://www.sciencedirect.com/science/article/pii/0378778888900266

[14] Bueno B, Norford L, Pigeon G, Britter R. A resistance-capacitance network model for the analysis of the interactions between the energy performance of buildings and the urban climate. Build Environ 2012;54:116–25. doi:10.1016/j.buildenv.2012.01.023. https://www.sciencedirect.com/science/article/pii/S0360132312000388

[15] Nouvel R, Brassel K-H, Bruse M, Duminil E, Coors V, Eicker U, ROBINSON D. SimStadt, a new workflow-driven urban energy simulation platform for CityGML city models. In: Proceedings of international conference CISBAT 2015 future buildings and districts sustainability from Nano to Urban Scale. LESO-PB, EPFL; 2015. p. 889–94. Issue: CONF

[16] Bueno B, Norford L, Hidalgo J, Pigeon G. The urban weather generator. J Build Perform Simul 2013;6(4):269–81. doi:10.1080/19401493.2012.718797. Publisher: Taylor & Francis _eprint: https://doi.org/10.1080/19401493.2012.718797

[17] Kusaka H, Kondo H, Kikegawa Y, Kimura F. A simple single-layer urban canopy model for atmospheric models: Comparison with multi-layer and slab models. Boundary Layer Meteorol 2001;101(3):329–58. doi:10.1023/A:1019207923078.

[18] Romero Rodríguez L, Sánchez Ramos J, Molina Félix JL, Álvarez Domínguez S. Urban-scale air temperature estimation: development of an empirical model based on mobile transects. Sustain Cities Soc 2020;63:102471. doi:10.1016/j.scs.2020.102471. https://www.sciencedirect.com/science/article/pii/S2210670720306910

[19] Hsu A, Sheriff G, Chakraborty T, Manya D. Disproportionate exposure to urban heat island intensity across major US cities. Nat Commun 2021;12(1):2721. doi:10.1038/s41467-021-22799-5. Number: 1 Publisher: Nature Publishing Group

[20] Allegrini J, Dorer V, Carmeliet J. Influence of morphologies on the microclimate in urban neighbourhoods. J Wind Eng Ind Aerodyn 2015;144:108–17. doi:10.1016/j.jweia.2015.03.024. https://www.sciencedirect.com/science/article/pii/S0167610515000896

[21] De Ridder K, Lauwaet D, Maiheu B. UrbClim – a fast urban boundary layer climate model. Urban Clim 2015;12:21–48. doi:10.1016/j.uclim.2015.01.001. https://www.sciencedirect.com/science/article/pii/S2212095515000024

[22] Dougherty TR, Jain RK. Invisible walls: exploration of microclimate effects on building energy consumption in New York City. Sustain Cities Soc 2023;90:104364. doi:10.1016/j.scs.2022.104364. https://www.sciencedirect.com/science/article/pii/S2210670722006692

[23] Mayer K, Haas L, Huang T, Bernabé-Moreno J, Rajagopal R, Fischer M. Estimating building energy efficiency from street view imagery, aerial imagery, and land surface temperature data. Appl Energy 2023;333:120542. doi:10.1016/j.apenergy.2022.120542. https://www.sciencedirect.com/science/article/pii/S0306261922017998

[24] Hong T, Xu Y, Sun K, Zhang W, Luo X, Hooper B. Urban microclimate and its impact on building performance: a case study of San Francisco. Urban Clim 2021;38:100871. doi:10.1016/j.uclim.2021.100871. https://www.sciencedirect.com/science/article/pii/S2212095521001012

[25] Bianchi C., Fontanini A.. TMY3 weather data for ComStock and ResStock.2021.

[26] Roth J., Bailey A., Choudhary S., Jain R.K.. Spatial and temporal modeling of urban building energy consumption using machine learning and open data2019;:459–467. Publisher: American Society of Civil Engineers; doi:10.1061/9780784482445.059.

[27] Blaom AD, Kiraly F, Lienart T, Simillides Y, Arenas D, Vollmer SJ. MLJ: a Julia package for composable machine learning. J Open Source Softw 2020;5(55):2704. doi:10.21105/joss.02704. Publisher: The Open Journal

[28] Urquhart M, Ljungskog E, Sebben S. Surrogate-based optimisation using adaptively scaled radial basis functions. Appl Soft Comput 2020;88. doi:10.1016/j.asoc.2019.106050.

[29] Landsberg DR, Shonder JA. ASHRAE guideline 14 cognizant TC: TC 7.6, building energy performance. SPLS; 2014.

[30] Lundberg SM, Lee S-I. A unified approach to interpreting model predictions. In: NIPS'17: Proceedings of the 31st international conference on neural information processing systems. Red Hook, NY, USA: Curran Associates Inc.; 2017. p. 4768–77. ISBN 978-1-5108-6096-4

[31] Štrumbelj E, Kononenko I. Explaining prediction models and individual predictions with feature contributions. Knowl Inf Syst 2014;41(3):647–65. doi:10.1007/s10115-013-0679-x.

[32] Winter E. Chapter 53 the shapley value. In: Handbook of game theory with economic applications, vol. 3. Elsevier; 2002. p. 2025–54. doi:10.1016/S1574-0005(02)03016-3. https://www.sciencedirect.com/science/article/pii/S1574000502030163

[33] Gabrielli P, Gazzani M, Martelli E, Mazzotti M. Optimal design of multi-energy systems with seasonal storage. Appl Energy 2018;219:408–24. doi:10.1016/j.apenergy.2017.07.142. https://www.sciencedirect.com/science/article/pii/S0306261917310139

[34] Ang YQ, Berzolla ZM, Reinhart CF. From concept to application: a review of use cases in urban building energy modeling. Appl Energy 2020;279:115738. doi:10.1016/j.apenergy.2020.115738. https://www.sciencedirect.com/science/article/pii/S0306261920312289

[35] Cui M. District heating load prediction algorithm based on bidirectional long short-term memory network model. Energy 2022;254:124283. doi:10.1016/j.energy.2022.124283. https://www.sciencedirect.com/science/article/pii/S0360544222011860

[36] Gabrielli P, Campos J, Becattini V, Mazzotti M, Sansavini G. Optimization and assessment of carbon capture, transport and storage supply chains for industrial sectors: the cost of resilience. Int J Greenhouse Gas Control 2022;121:103797. doi:10.1016/j.ijggc.2022.103797. https://www.sciencedirect.com/science/article/pii/S1750583622002158

[37] Makhmalbaf A, Fuller JC, Srivastava V, Ciraci S, Daily JA. Co-simulation of detailed whole building with the power system to study smart grid applications. Tech. Rep. PNNL-SA-103208. IEEE, Piscatawy, NJ, United States(US); 2014. doi:101109/SusTech20147046242. https://www.osti.gov/biblio/1172465

[38] Nouvel R, Mastrucci A, Leopold U, Baume O, Coors V, Eicker U. Combining GIS-based statistical and engineering urban heat consumption models: towards a new framework for multi-scale policy support. Energy Build 2015;107:204–12. doi:10.1016/j.enbuild.2015.08.021. https://www.sciencedirect.com/science/article/pii/S0378778815302061

[39] Streltsov A, Malof JM, Huang B, Bradbury K. Estimating residential building energy consumption using overhead imagery. Appl Energy 2020;280:116018. doi:10.1016/j.apenergy.2020.116018. https://www.sciencedirect.com/science/article/pii/S0306261920314616

[40] Wang Z, Hong T, Li H, Ann Piette M. Predicting city-scale daily electricity consumption using data-driven models. Adv. Appl. Energy 2021;2:100025. doi:10.1016/j.adapen.2021.100025. https://www.sciencedirect.com/science/article/pii/S2666792421000184

[41] Liu D, Wang W, Liu J. Sensitivity analysis of meteorological parameters on building energy consumption. Energy Procedia 2017;132:634–9. doi:10.1016/j.egypro.2017.09.700. https://www.sciencedirect.com/science/article/pii/S1876610217348476

[42] Hadavi M, Pasdarshahri H. Impacts of urban buildings on microclimate and cooling systems efficiency: coupled CFD and BES simulations. Sustain Cities Soc 2021;67:102740. doi:10.1016/j.scs.2021.102740. https://www.sciencedirect.com/science/article/pii/S2210670721000354

[43] Gamba P, Aldrighi M. SAR data classification of urban areas by means of segmentation techniques and ancillary optical data. IEEE J Sel Top Appl Earth Obs Remote Sens 2012;5(4):1140–8. doi:10.1109/JSTARS.2012.2195774. Conference Name: IEEE Journal of Selected Topics in Applied Earth Observations and Remote Sensing

[44] Kumar D. Urban objects detection from C-band synthetic aperture radar (SAR) satellite images through simulating filter properties. Sci Rep 2021;11(1):6241. doi:10.1038/s41598-021-85121-9. Number: 1 Publisher: Nature Publishing Group

[45] Dougherty TR, Huang T, Chen Y, Jain RK, Rajagopal R. SCHMEAR: scalable construction of holistic models for energy analysis from rooftops. In: BuildSys '21: Proceedings of the 8th ACM International Conference on Systems for Energy-Efficient Buildings, Cities, and Transportation. New York, NY, USA: Association for Computing Machinery; 2021. p. 111–20. doi:10.1145/3486611.3486666. ISBN 978-1-4503-9114-6